Chapter 14
Dual Craig-Bampton Method with Reduction of Interface Coordinates

Fabian M. Gruber, Tim L. Bürchner, and Daniel Jean Rixen

Abstract Dynamic substructuring techniques divide large models into substructures whereby each substructure is reduced and then assembled into a reduced model of low order which approximates the behaviour of the original model. Thereby the boundary degrees of freedom (degrees of freedom shared with adjacent substructures) are kept and only the internal degrees of freedom of each substructure are reduced to a small number of generalized coordinates.

If the interfaces between the substructures are large or if many substructures are used, the number of interface degrees of freedom is high. In that case the boundary degrees of freedom form a large subset of the generalized coordinates of the reduced substructures, which often is not necessary for the accurate description of the overall dynamics, but is present just for the interface assembly. To overcome this drawback and get a reduced model of low order, the interface degrees of freedom have to be reduced as well.

In this contribution, the reduction of interface coordinates for the dual Craig-Bampton method is demonstrated. The dual Craig-Bampton method employs free-interface vibration modes together with attachment modes to build the reduction bases of the substructures and assembles the substructures using interface forces (dual assembly). Considering the interface problem, a static reduction (Guyan reduction) of the interface coordinates is derived to obtain interface modes for the approximation of the interface degrees of freedom. Further, a reduction of interface coordinates using interface normal modes is demonstrated. The approximation accuracy of the different interface reduction approaches is evaluated. Focus will be directed to the influence on the negative eigenvalues of the reduced system which are intrinsic to the dual Craig-Bampton method. The proposed approach will be illustrated on examples where interface modes can be visualized in order to analyze their influence on the approximation quality of the reduced system.

Keywords Dynamic substructuring • Component mode synthesis • Dual Craig-Bampton method • Free interface method • Interface reduction • Interface modes

14.1 Introduction

The increasing performance of modern computers makes it possible to solve very large linear systems of millions of degrees of freedom (DOFs) very fast. Nevertheless, since the refinement of finite element models is increasing faster than the computing capabilities, dynamic substructuring still remains an essential tool for analyzing dynamical systems in an efficient manner. Building reduced models of submodels of a structure enables sharing models between design groups. Moreover the reduction of the DOFs of substructures is also important for building reduced order models for optimization and control. If a single component of a system is changed, only that component needs to be reanalyzed and the system can be analyzed at low additional cost. Thus dynamic substructuring offers a flexible and efficient approach to dynamic analysis [1, 2, 4, 6, 8, 9, 12, 13].

Dynamic substructuring techniques can be classified in two categories depending on the underlying modes which are used [1]. The term mode can refer to all kind of structural shape vectors. The first class consists of methods using fixed interface vibration modes and interface constraint modes to represent the substructure dynamics. The method commonly used is the Craig-Bampton method [2] which assembles the substructures in a primal way using interface displacements in order to enforce interface compatibility. The second class consists of methods using free interface vibration modes and

F.M. Gruber (✉) • T.L. Bürchner
Chair of Applied Mechanics, Faculty of Mechanical Engineering, Technical University of Munich, Boltzmannstr. 15, 85748, Garching, Germany
e-mail: fabian.gruber@tum.de; tim.buerchner@tum.de

D.J. Rixen
Technical University of Munich, Boltzmannstraße 15, D-85748, Garching, Germany
e-mail: rixen@tum.de

M.S. Allen et al. (eds.), *Dynamics of Coupled Structures, Volume 4*, Conference Proceedings of the Society for Experimental Mechanics Series, DOI 10.1007/978-3-319-54930-9_14

attachment modes. Representatives of that class are MacNeal's method [8] and Rubin's method [12] using a primal assembly process as well. In contrast to the aforementioned methods, the dual Craig-Bampton method (DCBM) [9] uses also free interface vibration modes and attachment modes, but assembles the substructures in a dual way using interface forces. As a consequence, the DCBM enforces only weak interface compatibility between the substructures, thereby avoiding interface locking problems as sometimes experienced in the primal assembly approaches. Furthermore, the DCBM leads to simpler reduced matrices compared to other free interface methods and the reduced matrices are sparse, similar to the classical Craig-Bampton matrices [9].

All methods divide the large model of a dynamical system into substructures, each substructure is reduced and then assembled into a reduced model of low order which approximate the behavior of the original large model. During this process the DOFs of each substructure are divided into internal DOFs (not shared with any adjacent substructure) and boundary DOFs (shared with adjacent substructures and therefore forming the interface degrees of freedom of the model). Most substructuring methods keep all boundary DOFs and the process only reduces the internal DOFs of each substructure to a small number of generalized coordinates.

As long as the number of interface DOFs is low these substructuring methods result in reduced models of low order that approximates the dynamic behavior of the original model with excellent accuracy. But if the interfaces are large or if many substructures are used the number of interface DOFs is high. In that case the boundary DOFs constitute a significant part of the generalized coordinates of the reduced substructures, which often are not necessary for the description of the overall dynamics, but merely enables convenient assembly of the substructures. To overcome this drawback and get a reduced model of low order, the interface degrees of freedom have to be reduced as well. For many substructuring methods, e.g. the Craig-Bampton method (1968), different approaches for the reduction of the interface coordinates were proposed [3]. Thereby commonly the interface problem is considered and the interface DOFs are represented by a reduced number of interface modes and corresponding generalized interface coordinates. In this contribution we intend to demonstrate the reduction of interface coordinates for the dual Craig-Bampton method [9] which enables the reduction of interface coordinates significantly without deteriorating the approximation accuracy in the low frequency range.

In Sect. 14.2, the original formulation and an alternative formulation of the dual Craig-Bampton method are presented and are compared. Following this, a static reduction (Guyan reduction) and a modal reduction of the interface coordinates are derived in Sect. 14.3. The properties of these interface reduction methods will be illustrated subsequently in detail in Sect. 14.4 using a two-dimensional solid plane stress problem. Subsection 14.4.3 tries to give some interpretation of the interface modes using a simple example. Finally we conclude with some general remarks in Sect. 14.5 and give an outlook on further research.

14.2 Governing Equations

Consider a finite element model of a global domain Ω. This domain Ω is divided into N non-overlapping substructures called $\Omega^{(s)}$ such that every node belongs to exactly one substructure except for the nodes on the interface boundaries. The linear/linearized equation of motion of one substructure s is written as

$$\boldsymbol{M}^{(s)}\ddot{\boldsymbol{u}}^{(s)} + \boldsymbol{K}^{(s)}\boldsymbol{u}^{(s)} = \boldsymbol{f}^{(s)} + \boldsymbol{g}^{(s)}, \quad s = 1, \ldots, N \tag{14.1}$$

where the superscript (s) is the label of the particular substructure. $\boldsymbol{M}^{(s)}$, $\boldsymbol{K}^{(s)}$ and $\boldsymbol{u}^{(s)}$ are the mass matrix, the stiffness matrix and the displacement vector of the substructure, respectively. $\boldsymbol{f}^{(s)}$ is the external force vector and $\boldsymbol{g}^{(s)}$ is the vector of reaction forces on the substructure due to its connection to adjacent substructures at its boundary DOFs $\boldsymbol{u}_b^{(s)}$. The local displacements vector $\boldsymbol{u}^{(s)}$ of each substructure is divided in local internal DOFs $\boldsymbol{u}_i^{(s)}$ and boundary DOFs $\boldsymbol{u}_b^{(s)}$.

One way to enforce the interface compatibility between the different substructures is to consider the interface connecting forces $\boldsymbol{g}^{(s)}$ as unknowns. These forces must be determined to satisfy the interface compatibility condition (displacement equality) and the local equation of motion of the substructures:

$$\sum_{s=1}^{N} \boldsymbol{B}^{(s)}\boldsymbol{u}^{(s)} = \boldsymbol{0} \tag{14.2}$$

$$\boldsymbol{M}^{(s)}\ddot{\boldsymbol{u}}^{(s)} + \boldsymbol{K}^{(s)}\boldsymbol{u}^{(s)} + \boldsymbol{B}^{(s)^T}\boldsymbol{\lambda} = \boldsymbol{f}^{(s)} \tag{14.3}$$

$\boldsymbol{B}^{(s)}$ is a signed Boolean matrix (constraint matrix) acting on the substructure DOFs $\boldsymbol{u}^{(s)}$. $\boldsymbol{B}^{(s)^T}\boldsymbol{\lambda}$ is representing the interconnecting forces between substructures which is corresponding to the negative interface reaction force vector $\boldsymbol{g}^{(s)}$

in Eq. (14.1) meaning

$$\boldsymbol{g}^{(s)} = -\boldsymbol{B}^{(s)^T}\boldsymbol{\lambda}, \tag{14.4}$$

and $\boldsymbol{\lambda}$ is the vector of all Lagrange multipliers acting on the interfaces which are the additional unknowns.

Using the block-diagonal matrices

$$\boldsymbol{M} = \begin{bmatrix} \boldsymbol{M}^{(1)} & & \boldsymbol{0} \\ & \ddots & \\ \boldsymbol{0} & & \boldsymbol{M}^{(N)} \end{bmatrix}, \quad \boldsymbol{K} = \begin{bmatrix} \boldsymbol{K}^{(1)} & & \boldsymbol{0} \\ & \ddots & \\ \boldsymbol{0} & & \boldsymbol{K}^{(N)} \end{bmatrix}, \tag{14.5}$$

the corresponding partitioned vectors and Boolean matrix

$$\boldsymbol{u} = \begin{bmatrix} \boldsymbol{u}^{(1)} \\ \vdots \\ \boldsymbol{u}^{(N)} \end{bmatrix}, \quad \boldsymbol{f} = \begin{bmatrix} \boldsymbol{f}^{(1)} \\ \vdots \\ \boldsymbol{f}^{(N)} \end{bmatrix}, \quad \boldsymbol{B} = \begin{bmatrix} \boldsymbol{B}^{(1)} \cdots \boldsymbol{B}^{(N)} \end{bmatrix}, \tag{14.6}$$

the substructure Eqs. (14.2) and (14.3) can be assembled as

$$\boldsymbol{M}_{dual}\begin{bmatrix} \ddot{\boldsymbol{u}} \\ \ddot{\boldsymbol{\lambda}} \end{bmatrix} + \boldsymbol{K}_{dual}\begin{bmatrix} \boldsymbol{u} \\ \boldsymbol{\lambda} \end{bmatrix} = \begin{bmatrix} \boldsymbol{M} & \boldsymbol{0} \\ \boldsymbol{0} & \boldsymbol{0} \end{bmatrix}\begin{bmatrix} \ddot{\boldsymbol{u}} \\ \ddot{\boldsymbol{\lambda}} \end{bmatrix} + \begin{bmatrix} \boldsymbol{K} & \boldsymbol{B}^T \\ \boldsymbol{B} & \boldsymbol{0} \end{bmatrix}\begin{bmatrix} \boldsymbol{u} \\ \boldsymbol{\lambda} \end{bmatrix} = \begin{bmatrix} \boldsymbol{f} \\ \boldsymbol{0} \end{bmatrix} = \boldsymbol{f}_{dual}. \tag{14.7}$$

In this hybrid formulation the Lagrange multipliers $\boldsymbol{\lambda}$ enforce the interface compatibility constraints and can be identified as interface forces [9].

14.2.1 Original Formulation of the Dual Craig-Bampton Method (DCBM)

Considering the equation of motion (14.3) of substructure s, every substructure can be seen as being excited by the interface connection forces and the external forces [9]. This indicates that the displacements of each substructure $\boldsymbol{u}^{(s)}$ can be expressed in terms of local static solutions $\boldsymbol{u}_{stat}^{(s)}$ and in terms of eigenmodes associated to the entire substructure matrices $\boldsymbol{K}^{(s)}$ and $\boldsymbol{M}^{(s)}$:

$$\boldsymbol{u}^{(s)} = \boldsymbol{u}_{stat}^{(s)} + \sum_{j=1}^{n^{(s)}-r^{(s)}} \boldsymbol{\theta}_j^{(s)}\eta_j^{(s)} \qquad \text{with} \qquad \boldsymbol{u}_{stat}^{(s)} = -\boldsymbol{K}^{(s)^+}\boldsymbol{B}^{(s)^T}\boldsymbol{\lambda} + \sum_{j=1}^{r^{(s)}} \boldsymbol{R}_j^{(s)}\alpha_j^{(s)}. \tag{14.8}$$

$n^{(s)}$ is the dimension of the local substructure problem and $\boldsymbol{K}^{(s)^+}$ is equal to the inverse of $\boldsymbol{K}^{(s)}$ if there are enough boundary conditions to prevent the substructure from floating when its interface with adjacent substructures is free [9]. If a substructure is floating, the generalized inverse $\boldsymbol{K}^{(s)^+}$ has to be used. $\boldsymbol{R}^{(s)}$ is the matrix containing the $r^{(s)}$ rigid body modes as columns which are mass orthonormalized. The vector $\boldsymbol{\alpha}^{(s)}$ contains the amplitudes $\alpha_j^{(s)}$ of the rigid body modes $\boldsymbol{R}^{(s)}$. The flexibility matrix $\boldsymbol{G}^{(s)}$ in inertia-relief format is computed from any generalized inverse $\boldsymbol{K}^{(s)^+}$ by projecting out the rigid body modes $\boldsymbol{R}^{(s)}$ using the inertia-relief projection matrix $\boldsymbol{P}^{(s)}$ which is defined as [4, 5]

$$\boldsymbol{P}^{(s)} = \boldsymbol{I}^{(s)} - \boldsymbol{M}^{(s)}\boldsymbol{R}^{(s)}\boldsymbol{R}^{(s)^T} \tag{14.9}$$

and therefore

$$\boldsymbol{G}^{(s)} = \boldsymbol{P}^{(s)^T}\boldsymbol{K}^{(s)^+}\boldsymbol{P}^{(s)}. \tag{14.10}$$

The vector $\boldsymbol{\eta}^{(s)}$ contains the amplitudes $\eta_j^{(s)}$ of the local eigenmodes $\boldsymbol{\theta}_j^{(s)}$ being eigensolutions of the generalized eigenproblem

$$\boldsymbol{K}^{(s)}\boldsymbol{\theta}_j^{(s)} = \omega_j^{(s)^2}\boldsymbol{M}^{(s)}\boldsymbol{\theta}_j^{(s)}. \tag{14.11}$$

These free interface normal modes $\boldsymbol{\theta}_j^{(s)}$ are also mass orthonormalized. An approximation is obtained by retaining only the first free interface normal modes $\boldsymbol{\theta}_j^{(s)}$ corresponding to the $n_\theta^{(s)}$ lowest eigenvalues $\omega_j^{(s)^2}$. Calling $\boldsymbol{\Theta}^{(s)}$ the matrix containing these eigenmodes, the approximation of the displacements $\boldsymbol{u}^{(s)}$ of the substructure is given by

$$\boldsymbol{u}^{(s)} \approx -\boldsymbol{G}^{(s)}\boldsymbol{B}^{(s)^T}\boldsymbol{\lambda} + \boldsymbol{R}^{(s)}\boldsymbol{\alpha}^{(s)} + \boldsymbol{\Theta}^{(s)}\boldsymbol{\eta}^{(s)}. \tag{14.12}$$

$\boldsymbol{\Theta}^{(s)}$ is satisfying

$$\boldsymbol{\Theta}^{(s)^T}\boldsymbol{K}^{(s)}\boldsymbol{\Theta}^{(s)} = \boldsymbol{\Omega}^{(s)^2} = \mathrm{diag}(\omega_j^{(s)^2}) \qquad \text{and} \qquad \boldsymbol{\Theta}^{(s)^T}\boldsymbol{M}^{(s)}\boldsymbol{\Theta}^{(s)} = \boldsymbol{I} \tag{14.13}$$

with $\boldsymbol{\Omega}^{(s)}$ being a diagonal matrix containing the remaining $n_\theta^{(s)}$ eigenvalues $\omega_j^{(s)}$. Since a part of the subspace spanned by $\boldsymbol{\Theta}^{(s)}$ is already included in $\boldsymbol{G}^{(s)}$ the residual flexibility matrix $\boldsymbol{G}_r^{(s)}$ can be used instead of the flexibility matrix $\boldsymbol{G}^{(s)}$, which is defined by

$$\boldsymbol{G}_r^{(s)} = \sum_{j=n_\theta^{(s)}+1}^{n^{(s)}-r^{(s)}} \frac{\boldsymbol{\theta}_j^{(s)}\boldsymbol{\theta}_j^{(s)^T}}{\omega_j^{(s)^2}} = \boldsymbol{G}^{(s)} - \sum_{j=1}^{n_\theta^{(s)}} \frac{\boldsymbol{\theta}_j^{(s)}\boldsymbol{\theta}_j^{(s)^T}}{\omega_j^{(s)^2}}. \tag{14.14}$$

Note that, by construction $\boldsymbol{G}_r^{(s)} = \boldsymbol{G}_r^{(s)^T}$, which is computed using the second equality in Eq. (14.14). For further properties of $\boldsymbol{G}_r^{(s)}$ see [9, 10]. As a result the approximation of one substructure writes

$$\boldsymbol{u}^{(s)} \approx -\boldsymbol{G}_r^{(s)}\boldsymbol{B}^{(s)^T}\boldsymbol{\lambda} + \boldsymbol{R}^{(s)}\boldsymbol{\alpha}^{(s)} + \boldsymbol{\Theta}^{(s)}\boldsymbol{\eta}^{(s)} = \begin{bmatrix}\boldsymbol{R}^{(s)} & \boldsymbol{\Theta}^{(s)} & -\boldsymbol{G}_r^{(s)}\boldsymbol{B}^{(s)^T}\end{bmatrix}\begin{bmatrix}\boldsymbol{\alpha}^{(s)}\\ \boldsymbol{\eta}^{(s)}\\ \boldsymbol{\lambda}\end{bmatrix}. \tag{14.15}$$

Assembling all substructures N in a dual fashion according to Eq. (14.7) by keeping the interface forces $\boldsymbol{\lambda}$ as unknowns, the entire structure can consequently be approximated by

$$\begin{bmatrix}\boldsymbol{u}\\ \boldsymbol{\lambda}\end{bmatrix} \approx \begin{bmatrix}\boldsymbol{R}^{(1)} & \boldsymbol{\Theta}^{(1)} & & & \boldsymbol{0} & \boldsymbol{0} & -\boldsymbol{G}_r^{(1)}\boldsymbol{B}^{(1)^T}\\ & & \ddots & \ddots & & & \vdots\\ \boldsymbol{0} & \boldsymbol{0} & & & \boldsymbol{R}^{(N)} & \boldsymbol{\Theta}^{(N)} & -\boldsymbol{G}_r^{(N)}\boldsymbol{B}^{(N)^T}\\ \boldsymbol{0} & \boldsymbol{0} & & & \boldsymbol{0} & \boldsymbol{0} & \boldsymbol{I}\end{bmatrix}\begin{bmatrix}\boldsymbol{\alpha}^{(1)}\\ \boldsymbol{\eta}^{(1)}\\ \vdots\\ \boldsymbol{\alpha}^{(N)}\\ \boldsymbol{\eta}^{(N)}\\ \boldsymbol{\lambda}\end{bmatrix} = \underbrace{\begin{bmatrix}\boldsymbol{R} & \boldsymbol{\Theta} & -\boldsymbol{G}_r\boldsymbol{B}^T\\ \boldsymbol{0} & \boldsymbol{0} & \boldsymbol{I}\end{bmatrix}}_{\boldsymbol{T}_{DCB}}\begin{bmatrix}\boldsymbol{\alpha}\\ \boldsymbol{\eta}\\ \boldsymbol{\lambda}\end{bmatrix}. \tag{14.16}$$

The approximation of the dynamic equations of the dual assembled system (14.7) is

$$\boldsymbol{M}_{DCB}\begin{bmatrix}\ddot{\boldsymbol{\alpha}}\\ \ddot{\boldsymbol{\eta}}\\ \ddot{\boldsymbol{\lambda}}\end{bmatrix} + \boldsymbol{K}_{DCB}\begin{bmatrix}\boldsymbol{\alpha}\\ \boldsymbol{\eta}\\ \boldsymbol{\lambda}\end{bmatrix} = \boldsymbol{f}_{DCB} \tag{14.17}$$

with

$$\boldsymbol{M}_{DCB} = \boldsymbol{T}_{DCB}^T\begin{bmatrix}\boldsymbol{M} & \boldsymbol{0}\\ \boldsymbol{0} & \boldsymbol{0}\end{bmatrix}\boldsymbol{T}_{DCB} = \begin{bmatrix}\boldsymbol{I} & \boldsymbol{0} & \boldsymbol{0}\\ \boldsymbol{0} & \boldsymbol{I} & \boldsymbol{0}\\ \boldsymbol{0} & \boldsymbol{0} & \boldsymbol{M}_r\end{bmatrix}, \quad \boldsymbol{M}_r = \boldsymbol{B}\boldsymbol{G}_r\boldsymbol{M}\boldsymbol{G}_r\boldsymbol{B}^T = \sum_{s=1}^{N}\boldsymbol{B}^{(s)}\boldsymbol{G}_r^{(s)}\boldsymbol{M}^{(s)}\boldsymbol{G}_r^{(s)}\boldsymbol{B}^{(s)^T}, \tag{14.18}$$

$$\boldsymbol{K}_{DCB} = \boldsymbol{T}_{DCB}^T \begin{bmatrix} \boldsymbol{K} & \boldsymbol{B}^T \\ \boldsymbol{B} & \boldsymbol{0} \end{bmatrix} \boldsymbol{T}_{DCB} = \begin{bmatrix} \boldsymbol{0} & \boldsymbol{0} & \boldsymbol{R}^T\boldsymbol{B}^T \\ \boldsymbol{0} & \boldsymbol{\Omega}^2 & \boldsymbol{\Theta}^T\boldsymbol{B}^T \\ \boldsymbol{B}\boldsymbol{R} & \boldsymbol{B}\boldsymbol{\Theta} & -\boldsymbol{F}_r \end{bmatrix}, \quad \boldsymbol{F}_r = \boldsymbol{B}\boldsymbol{G}_r\boldsymbol{B}^T = \sum_{s=1}^{N} \boldsymbol{B}^{(s)}\boldsymbol{G}_r^{(s)}\boldsymbol{B}^{(s)^T}, \tag{14.19}$$

$$\boldsymbol{f}_{DCB} = \boldsymbol{T}_{DCB}^T \begin{bmatrix} \boldsymbol{f} \\ \boldsymbol{0} \end{bmatrix}. \tag{14.20}$$

The DCBM reduced system has the final size $n_{DCB} = n_{rig} + \sum_{s=1}^{N} n_\theta^{(s)} + n_\lambda$ with n_{rig} being the number of rigid body modes of all substructures, $n_\theta^{(s)}$ the number of free interface normal modes of substructure s and n_λ the number of Lagrange multipliers [9].

14.2.2 Alternative Formulation of the Dual Craig-Bampton Method

The original formulation of the DCBM [9] (see Sect. 14.2.1) uses residual attachment modes which are the columns of the residual flexibility matrix $\boldsymbol{G}_r^{(s)}$ and the reduced matrices in Eqs. (14.18) and (14.19) are resulting [11]. The coupling between residual attachment modes and free interface normal modes is contained in the reduced stiffness matrix $\boldsymbol{K}_{DCB}$. In the following an alternative formulation of the dual Craig-Bampton method [11] is recalled using attachment modes which are columns of the flexibility matrix $\boldsymbol{G}^{(s)}$, instead of residual attachment modes. This shifts the coupling between attachment modes and free interface normal modes to the reduced mass matrix which is beneficial for the computation of interface modes used afterwards for the reduction the interface coordinates. Assembling all substructures N which are approximated by Eq. (14.12) instead of Eq. (14.15), the entire structure can consequently be approximated by

$$\begin{bmatrix} \boldsymbol{u} \\ \boldsymbol{\lambda} \end{bmatrix} \approx \begin{bmatrix} \boldsymbol{R}^{(1)} & \boldsymbol{\Theta}^{(1)} & & & \boldsymbol{0} & \boldsymbol{0} & -\boldsymbol{G}^{(1)}\boldsymbol{B}^{(1)^T} \\ & & \ddots & \ddots & & & \vdots \\ \boldsymbol{0} & \boldsymbol{0} & & & \boldsymbol{R}^{(N)} & \boldsymbol{\Theta}^{(N)} & -\boldsymbol{G}^{(N)}\boldsymbol{B}^{(N)^T} \\ \boldsymbol{0} & \boldsymbol{0} & & & \boldsymbol{0} & \boldsymbol{0} & \boldsymbol{I} \end{bmatrix} \begin{bmatrix} \boldsymbol{\alpha}^{(1)} \\ \boldsymbol{\eta}^{(1)} \\ \vdots \\ \boldsymbol{\alpha}^{(N)} \\ \boldsymbol{\eta}^{(N)} \\ \boldsymbol{\lambda} \end{bmatrix} = \underbrace{\begin{bmatrix} \boldsymbol{R} & \boldsymbol{\Theta} & -\boldsymbol{G}\boldsymbol{B}^T \\ \boldsymbol{0} & \boldsymbol{0} & \boldsymbol{I} \end{bmatrix}}_{\bar{\boldsymbol{T}}_{DCB}} \begin{bmatrix} \boldsymbol{\alpha} \\ \boldsymbol{\eta} \\ \boldsymbol{\lambda} \end{bmatrix}. \tag{14.21}$$

The approximation of the dynamic equations of the dual assembled system (14.7) corresponding to the alternative formulation of the DCBM is

$$\bar{\boldsymbol{M}}_{DCB} \begin{bmatrix} \ddot{\boldsymbol{\alpha}} \\ \ddot{\boldsymbol{\eta}} \\ \ddot{\boldsymbol{\lambda}} \end{bmatrix} + \bar{\boldsymbol{K}}_{DCB} \begin{bmatrix} \boldsymbol{\alpha} \\ \boldsymbol{\eta} \\ \boldsymbol{\lambda} \end{bmatrix} = \bar{\boldsymbol{f}}_{DCB} \tag{14.22}$$

with

$$\bar{\boldsymbol{M}}_{DCB} = \bar{\boldsymbol{T}}_{DCB}^T \begin{bmatrix} \boldsymbol{M} & \boldsymbol{0} \\ \boldsymbol{0} & \boldsymbol{0} \end{bmatrix} \bar{\boldsymbol{T}}_{DCB} = \begin{bmatrix} \boldsymbol{I} & \boldsymbol{0} & \boldsymbol{0} \\ \boldsymbol{0} & \boldsymbol{I} & -\boldsymbol{\Omega}^{-2}\boldsymbol{\Theta}^T\boldsymbol{B}^T \\ \boldsymbol{0} & -\boldsymbol{B}\boldsymbol{\Theta}\boldsymbol{\Omega}^{-2} & \bar{\boldsymbol{M}}_r \end{bmatrix}, \tag{14.23}$$

$$\bar{\boldsymbol{M}}_r = \boldsymbol{B}\boldsymbol{G}\boldsymbol{M}\boldsymbol{G}\boldsymbol{B}^T = \sum_{s=1}^{N} \boldsymbol{B}^{(s)}\boldsymbol{G}^{(s)}\boldsymbol{M}^{(s)}\boldsymbol{G}^{(s)}\boldsymbol{B}^{(s)^T}, \tag{14.24}$$

$$\bar{\boldsymbol{K}}_{DCB} = \bar{\boldsymbol{T}}_{DCB}^T \begin{bmatrix} \boldsymbol{K} & \boldsymbol{B}^T \\ \boldsymbol{B} & \boldsymbol{0} \end{bmatrix} \bar{\boldsymbol{T}}_{DCB} = \begin{bmatrix} \boldsymbol{0} & \boldsymbol{0} & \boldsymbol{R}^T\boldsymbol{B}^T \\ \boldsymbol{0} & \boldsymbol{\Omega}^2 & \boldsymbol{0} \\ \boldsymbol{B}\boldsymbol{R} & \boldsymbol{0} & -\bar{\boldsymbol{F}}_r \end{bmatrix}, \quad \bar{\boldsymbol{F}}_r = \boldsymbol{B}\boldsymbol{G}\boldsymbol{B}^T = \sum_{s=1}^{N} \boldsymbol{B}^{(s)}\boldsymbol{G}^{(s)}\boldsymbol{B}^{(s)^T}, \tag{14.25}$$

$$\bar{\boldsymbol{f}}_{DCB} = \begin{bmatrix} \boldsymbol{f} \\ \boldsymbol{0} \end{bmatrix}. \tag{14.26}$$

The final size of the reduced system using the alternative formulation of the DCBM is obviously the same as for the original formulation.

14.2.3 Comparison of the Two Formulations of the Dual Craig-Bampton Method

Equation (14.27) repeats the reduced equations of motion obtained by applying the original formulation of the DCBM [9] and Eq. (14.28) the reduced equations of motion obtained by applying the alternative formulation of the DCBM [11]:

$$\begin{bmatrix} \boldsymbol{I} & \boldsymbol{0} & \boldsymbol{0} \\ \boldsymbol{0} & \boldsymbol{I} & \boldsymbol{0} \\ \boldsymbol{0} & \boldsymbol{0} & \boldsymbol{M}_r \end{bmatrix} \begin{bmatrix} \ddot{\boldsymbol{\alpha}} \\ \ddot{\boldsymbol{\eta}} \\ \ddot{\boldsymbol{\lambda}} \end{bmatrix} + \begin{bmatrix} \boldsymbol{0} & \boldsymbol{0} & \boldsymbol{R}^T\boldsymbol{B}^T \\ \boldsymbol{0} & \boldsymbol{\Omega}^2 & \boldsymbol{\Theta}^T\boldsymbol{B}^T \\ \boldsymbol{BR} & \boldsymbol{B\Theta} & -\boldsymbol{F}_r \end{bmatrix} \begin{bmatrix} \boldsymbol{\alpha} \\ \boldsymbol{\eta} \\ \boldsymbol{\lambda} \end{bmatrix} = \boldsymbol{T}_{DCB}^T \begin{bmatrix} \boldsymbol{f} \\ \boldsymbol{0} \end{bmatrix} \tag{14.27}$$

$$\begin{bmatrix} \boldsymbol{I} & \boldsymbol{0} & \boldsymbol{0} \\ \boldsymbol{0} & \boldsymbol{I} & -\boldsymbol{\Omega}^{-2}\boldsymbol{\Theta}^T\boldsymbol{B}^T \\ \boldsymbol{0} & -\boldsymbol{B\Theta}\boldsymbol{\Omega}^{-2} & \bar{\boldsymbol{M}}_r \end{bmatrix} \begin{bmatrix} \ddot{\boldsymbol{\alpha}} \\ \ddot{\boldsymbol{\eta}} \\ \ddot{\boldsymbol{\lambda}} \end{bmatrix} + \begin{bmatrix} \boldsymbol{0} & \boldsymbol{0} & \boldsymbol{R}^T\boldsymbol{B}^T \\ \boldsymbol{0} & \boldsymbol{\Omega}^2 & \boldsymbol{0} \\ \boldsymbol{BR} & \boldsymbol{0} & -\bar{\boldsymbol{F}}_r \end{bmatrix} \begin{bmatrix} \boldsymbol{\alpha} \\ \boldsymbol{\eta} \\ \boldsymbol{\lambda} \end{bmatrix} = \bar{\boldsymbol{T}}_{DCB}^T \begin{bmatrix} \boldsymbol{f} \\ \boldsymbol{0} \end{bmatrix} \tag{14.28}$$

The reduced matrices of Eqs. (14.27) and (14.28) of the two formulations are different but it should be noted that the reduction basis and the dual assembly procedure is the same for both formulations [11]. Therefore both formulations are mathematically equivalent and will give the same results. Using residual attachment modes, the coupling between these modes and the free interface normal modes appears in the stiffness matrix. As opposed to this, using attachment modes the coupling between the attachment modes and the free interface modes appears in the mass matrix.

One important fact used later for the interface reduction is that the subpart of the reduced matrices of the alternative formulation

$$\begin{bmatrix} \boldsymbol{I} & \boldsymbol{0} \\ \boldsymbol{0} & \bar{\boldsymbol{M}}_r \end{bmatrix} \begin{bmatrix} \ddot{\boldsymbol{\alpha}} \\ \ddot{\boldsymbol{\lambda}} \end{bmatrix} + \begin{bmatrix} \boldsymbol{0} & \boldsymbol{R}^T\boldsymbol{B}^T \\ \boldsymbol{BR} & -\bar{\boldsymbol{F}}_r \end{bmatrix} \begin{bmatrix} \boldsymbol{\alpha} \\ \boldsymbol{\lambda} \end{bmatrix} = \begin{bmatrix} \boldsymbol{R}^T\boldsymbol{f} \\ -\boldsymbol{BGf} \end{bmatrix}, \tag{14.29}$$

which corresponds to the rigid body modes and the attachment modes, does not change when the number of free interface normal modes retained in the reduction basis $n_\theta = \sum_{s=1}^{N} n_\theta^{(s)}$ is changed. This is due to the flexibility matrix $\boldsymbol{G}$, which is implicitly included in $\bar{\boldsymbol{M}}_r$ and $\bar{\boldsymbol{F}}_r$, being independent on the number of free interface normal modes n_θ retained in the reduction basis. That is not the case for the original formulation of the DCBM (see Sect. 14.2.1) since the subspace spanned by the free interface normal modes $\boldsymbol{\Theta}$ according to Eq. (14.14) is projected out of the flexibility matrix $\boldsymbol{G}$ to obtain the residual flexibility matrix $\boldsymbol{G}_r$. This makes $\boldsymbol{G}_r$ dependent on $\boldsymbol{\Theta}$ and therefore $\boldsymbol{G}_r$ is changing if $\boldsymbol{\Theta}$ is changed. Consequently $\boldsymbol{F}_r$ and $\boldsymbol{M}_r$ are also changing in that case since $\boldsymbol{F}_r$ and $\boldsymbol{M}_r$ depend again on $\boldsymbol{G}_r$ as can be seen in Eqs. (14.18) and (14.19).

14.3 Reduction of Interface Coordinates

Using the DCBM (it does not matter which formulation) the number of Lagrange multipliers n_λ and also the number rigid body modes n_{rig} remains constant during the reduction process. The size of the interface problem $n_{int} = n_\lambda + n_{rig}$ is not affected by the DCBM reduction. If the number of substructures increases the size of the corresponding interface problem increases, so that for a large number of substructures the reduced system can still have a significant number of DOFs. For the Craig-Bampton method [2] different reduction methods were proposed in [3], namely "Modal reduction of junction coordinates", "Guyan reduction of junction coordinates" and "Ritz reduction of junction coordinates" (which is the most general case including the first two techniques as special cases). These techniques consist in representing the interface DOFs in terms of a reduced number of modes with corresponding generalized interface mode coordinates. In order to reduce the interface problem of the DCBM we want to demonstrate a Guyan reduction and a modal reduction of the interface coordinates of the DCBM in the following.

Therefore we consider the interface problem for the DCBM which is obtained by static condensation (no free vibration modes are included in the reduction basis) of the dual assembled problem (14.7). The static reduction

$$\begin{bmatrix} \boldsymbol{u} \\ \boldsymbol{\lambda} \end{bmatrix} \approx \underbrace{\begin{bmatrix} \boldsymbol{R} & -\boldsymbol{GB}^T \\ \boldsymbol{0} & \boldsymbol{I} \end{bmatrix}}_{\boldsymbol{T}_{stat}} \begin{bmatrix} \boldsymbol{\alpha} \\ \boldsymbol{\lambda} \end{bmatrix}, \tag{14.30}$$

which is obtain by deleting the column corresponding to $\boldsymbol{\Theta}$ in $\bar{\boldsymbol{T}}_{DCB}$ of Eq. (14.21) resulting in the static reduction matrix $\boldsymbol{T}_{stat}$ gives the interface problem

$$\begin{bmatrix} \boldsymbol{I} & \boldsymbol{0} \\ \boldsymbol{0} & \bar{\boldsymbol{M}}_r \end{bmatrix} \begin{bmatrix} \ddot{\boldsymbol{\alpha}} \\ \ddot{\boldsymbol{\lambda}} \end{bmatrix} + \begin{bmatrix} \boldsymbol{0} & \boldsymbol{R}^T\boldsymbol{B}^T \\ \boldsymbol{BR} & -\bar{\boldsymbol{F}}_r \end{bmatrix} \begin{bmatrix} \boldsymbol{\alpha} \\ \boldsymbol{\lambda} \end{bmatrix} = \begin{bmatrix} \boldsymbol{R}^T\boldsymbol{f} \\ -\boldsymbol{BGf} \end{bmatrix} \tag{14.31}$$

with the mass matrix $\boldsymbol{M}_{int}$ and stiffness matrix $\boldsymbol{K}_{int}$ of the interface problem:

$$\boldsymbol{M}_{int} = \boldsymbol{T}_{stat}^T \begin{bmatrix} \boldsymbol{M} & \boldsymbol{0} \\ \boldsymbol{0} & \boldsymbol{0} \end{bmatrix} \boldsymbol{T}_{stat} = \begin{bmatrix} \boldsymbol{I} & \boldsymbol{0} \\ \boldsymbol{0} & \bar{\boldsymbol{M}}_r \end{bmatrix}, \qquad \boldsymbol{K}_{int} = \boldsymbol{T}_{stat}^T \begin{bmatrix} \boldsymbol{K} & \boldsymbol{B}^T \\ \boldsymbol{B} & \boldsymbol{0} \end{bmatrix} \boldsymbol{T}_{stat} = \begin{bmatrix} \boldsymbol{0} & \boldsymbol{R}^T\boldsymbol{B}^T \\ \boldsymbol{BR} & -\bar{\boldsymbol{F}}_r \end{bmatrix} \tag{14.32}$$

Note that is does no matter if either the original formulation of the DCBM or the alternative formulation of the DCBM is used to obtain this static problem since when no vibration modes are kept the (residual) flexibility matrices $\boldsymbol{G}_r = \boldsymbol{G}$ are equal [11].

14.3.1 Guyan Reduction of Interface Coordinates

Analogously to the Craig-Bampton method with Guyan reduction of interface coordinates [3], now the Lagrange multipliers $\boldsymbol{\lambda}$ are divided in kept $\boldsymbol{\lambda}_k$ and approximated $\boldsymbol{\lambda}_a$ DOFs. The rigid body modes $\boldsymbol{\alpha}$ are kept in any case. By reordering Eq. (14.31), the partitioned interface problem for free vibration writes

$$\begin{bmatrix} \boldsymbol{M}_{int,\alpha\alpha} & \boldsymbol{0} & \boldsymbol{0} \\ \boldsymbol{0} & \boldsymbol{M}_{int,\lambda_k\lambda_k} & \boldsymbol{M}_{int,\lambda_k\lambda_a} \\ \boldsymbol{0} & \boldsymbol{M}_{int,\lambda_a\lambda_k} & \boldsymbol{M}_{int,\lambda_a\lambda_a} \end{bmatrix} \begin{bmatrix} \ddot{\boldsymbol{\alpha}} \\ \ddot{\boldsymbol{\lambda}}_k \\ \ddot{\boldsymbol{\lambda}}_a \end{bmatrix} + \begin{bmatrix} \boldsymbol{0} & \boldsymbol{K}_{int,\alpha\lambda_k} & \boldsymbol{K}_{int,\alpha\lambda_a} \\ \boldsymbol{K}_{int,\lambda_k\alpha} & \boldsymbol{K}_{int,\lambda_k\lambda_k} & \boldsymbol{K}_{int,\lambda_k\lambda_a} \\ \boldsymbol{K}_{int,\lambda_a\alpha} & \boldsymbol{K}_{int,\lambda_a\lambda_k} & \boldsymbol{K}_{int,\lambda_a\lambda_a} \end{bmatrix} \begin{bmatrix} \boldsymbol{\alpha} \\ \boldsymbol{\lambda}_k \\ \boldsymbol{\lambda}_a \end{bmatrix} = \begin{bmatrix} \boldsymbol{0} \\ \boldsymbol{0} \\ \boldsymbol{0} \end{bmatrix}. \tag{14.33}$$

Solving the third row of the static problem (14.33)

$$\boldsymbol{K}_{int,\lambda_a\alpha}\boldsymbol{\alpha} + \boldsymbol{K}_{int,\lambda_a\lambda_k}\boldsymbol{\lambda}_k + \boldsymbol{K}_{int,\lambda_a\lambda_a}\boldsymbol{\lambda}_a = \boldsymbol{0}, \tag{14.34}$$

the approximated DOFs $\boldsymbol{\lambda}_a$ are obtained by

$$\boldsymbol{\lambda}_a = -\boldsymbol{K}_{int,\lambda_a\lambda_a}^{-1}\boldsymbol{K}_{int,\lambda_a\alpha}\boldsymbol{\alpha} - \boldsymbol{K}_{int,\lambda_a\lambda_a}^{-1}\boldsymbol{K}_{int,\lambda_a\lambda_k}\boldsymbol{\lambda}_k = \boldsymbol{\Psi}_{ak,\alpha}\boldsymbol{\alpha} + \boldsymbol{\Psi}_{ak,\lambda}\boldsymbol{\lambda}_k. \tag{14.35}$$

This leads to the Guyan interface reduction matrix $\boldsymbol{T}_{DCB,Guyan}$

$$\begin{bmatrix} \boldsymbol{\alpha} \\ \boldsymbol{\eta} \\ \boldsymbol{\lambda}_k \\ \boldsymbol{\lambda}_a \end{bmatrix} \approx \underbrace{\begin{bmatrix} \boldsymbol{I} & \boldsymbol{0} & \boldsymbol{0} \\ \boldsymbol{0} & \boldsymbol{I} & \boldsymbol{0} \\ \boldsymbol{0} & \boldsymbol{0} & \boldsymbol{I} \\ \boldsymbol{\Psi}_{ak,\alpha} & \boldsymbol{0} & \boldsymbol{\Psi}_{ak,\lambda} \end{bmatrix}}_{\boldsymbol{T}_{DCB,Guyan}} \begin{bmatrix} \boldsymbol{\alpha} \\ \boldsymbol{\eta} \\ \boldsymbol{\lambda}_k \end{bmatrix}. \tag{14.36}$$

The dynamic equation with Guyan reduction of interface coordinates writes

$$\boldsymbol{M}_{DCB,Guyan}\ddot{\boldsymbol{u}}_{DCB,Guyan} + \boldsymbol{K}_{DCB,Guyan}\boldsymbol{u}_{DCB,Guyan} = \boldsymbol{f}_{DCB,Guyan} \tag{14.37}$$

with

$$\boldsymbol{M}_{DCB,Guyan} = \boldsymbol{T}_{DCB,Guyan}^T\bar{\boldsymbol{M}}_{DCB}\boldsymbol{T}_{DCB,Guyan} = \boldsymbol{T}_{DCB,Guyan}^T\bar{\boldsymbol{T}}_{DCB}^T\boldsymbol{M}_{dual}\bar{\boldsymbol{T}}_{DCB}\boldsymbol{T}_{DCB,Guyan}\,, \tag{14.38}$$

$$\boldsymbol{K}_{DCB,Guyan} = \boldsymbol{T}_{DCB,Guyan}^T\bar{\boldsymbol{K}}_{DCB}\boldsymbol{T}_{DCB,Guyan} = \boldsymbol{T}_{DCB,Guyan}^T\bar{\boldsymbol{T}}_{DCB}^T\boldsymbol{K}_{dual}\bar{\boldsymbol{T}}_{DCB}\boldsymbol{T}_{DCB,Guyan}\,, \tag{14.39}$$

$$\boldsymbol{u}_{DCB,Guyan} = \begin{bmatrix} \boldsymbol{\alpha} \\ \boldsymbol{\eta} \\ \boldsymbol{\lambda}_k \end{bmatrix}, \qquad \boldsymbol{f}_{DCB,Guyan} = \boldsymbol{T}_{DCB,Guyan}^T \bar{\boldsymbol{f}}_{DCB} = \boldsymbol{T}_{DCB,Guyan}^T \bar{\boldsymbol{T}}_{DCB}^T \boldsymbol{f}_{dual} \,. \tag{14.40}$$

A criterion for the choice of the kept Lagrange multipliers $\boldsymbol{\lambda}_k$ is the quotient K_{jj}/M_{jj} of the diagonal entries of the stiffness and mass matrix [3] with the coordinates having smaller K_{jj}/M_{jj} values being kept. This ensures keeping all rigid body modes, as stated before, since their corresponding quotient would be zero. The final size of a DCBM reduced system with Guyan interface reduction is $n_{DCB,Guyan} = n_{rig} + \sum_{s=1}^{N} n_\theta^{(s)} + n_{\lambda_k}$, with n_{rig} being the number of rigid body modes of all substructures, $n_\theta^{(s)}$ the number of free interface normal modes of substructure s and n_{λ_k} the number of kept Lagrange multipliers.

14.3.2 Modal Reduction of Interface Coordinates

An approach for the modal reduction of interface coordinates of the DCBM was first given in [11]. As for the Guyan interface reduction (Sect. 14.3.1) the starting point for the following derivation is the statically condensed dual problem (14.31) which is equivalent to a DCBM reduction with no free interface vibration modes included in the reduction basis. The DCBM interface modes $\boldsymbol{x}_{int,j}$ are eigensolutions of that statically condensed dual interface problem

$$\boldsymbol{K}_{int}\boldsymbol{x}_{int,j} = \mu_k^2 \boldsymbol{M}_{int}\boldsymbol{x}_{int,j} \qquad \Leftrightarrow \qquad \begin{bmatrix} \boldsymbol{0} & \boldsymbol{R}^T\boldsymbol{B}^T \\ \boldsymbol{B}\boldsymbol{R} & -\bar{\boldsymbol{F}}_{res} \end{bmatrix} \begin{bmatrix} \boldsymbol{x}_{\alpha,j} \\ \boldsymbol{x}_{\lambda,j} \end{bmatrix} = \mu_j^2 \begin{bmatrix} \boldsymbol{I} & \boldsymbol{0} \\ \boldsymbol{0} & \bar{\boldsymbol{M}}_{res} \end{bmatrix} \begin{bmatrix} \boldsymbol{x}_{\alpha,j} \\ \boldsymbol{x}_{\lambda,j} \end{bmatrix}. \tag{14.41}$$

These interface modes $\boldsymbol{x}_{int,j}$ are mass orthonormalized and an approximation of the interface coordinates is obtained by retaining only the first interface modes $\boldsymbol{x}_{int,j}$ corresponding to the n_x lowest eigenvalues μ_j^2. Calling

$$\boldsymbol{X}_{int} = \begin{bmatrix} \boldsymbol{X}_\alpha \\ \boldsymbol{X}_\lambda \end{bmatrix} \tag{14.42}$$

the matrix containing these n_x interface modes, the approximation of the interface DOFs is given by

$$\begin{bmatrix} \boldsymbol{\alpha} \\ \boldsymbol{\lambda} \end{bmatrix} \approx \boldsymbol{X}_{int}\tilde{\boldsymbol{\lambda}} = \begin{bmatrix} \boldsymbol{X}_\alpha \\ \boldsymbol{X}_\lambda \end{bmatrix} \tilde{\boldsymbol{\lambda}} \tag{14.43}$$

which leads to the modal interface reduction matrix $\boldsymbol{T}_{DCB,modal}$

$$\begin{bmatrix} \boldsymbol{\alpha} \\ \boldsymbol{\eta} \\ \boldsymbol{\lambda} \end{bmatrix} \approx \underbrace{\begin{bmatrix} \boldsymbol{0} & \boldsymbol{X}_\alpha \\ \boldsymbol{I} & \boldsymbol{0} \\ \boldsymbol{0} & \boldsymbol{X}_\lambda \end{bmatrix}}_{\boldsymbol{T}_{DCB,modal}} \begin{bmatrix} \boldsymbol{\eta} \\ \tilde{\boldsymbol{\lambda}} \end{bmatrix}. \tag{14.44}$$

$\boldsymbol{X}_{int}$ is satisfying

$$\boldsymbol{X}_{int}\boldsymbol{K}_{int}\boldsymbol{X}_{int} = \boldsymbol{\mu}^2 = \mathrm{diag}(\mu_j^2) \qquad \text{and} \qquad \boldsymbol{X}_{int}\boldsymbol{M}_{int}\boldsymbol{X}_{int} = \boldsymbol{I} \tag{14.45}$$

with $\boldsymbol{\mu}^2$ being a diagonal matrix containing the remaining n_x eigenvalues μ_j^2. The vector $\tilde{\boldsymbol{\lambda}}$ contains the amplitudes $\tilde{\lambda}_j$ of the retained interface modes $\boldsymbol{x}_{int,j}$ and the modal parameters $\boldsymbol{\eta}$ are not affected by the approximation (14.44). Applying the reduction (14.44) to the DCBM reduced system (14.22), the dynamic equation with modal reduction of interface coordinates writes

$$\boldsymbol{M}_{DCB,modal}\ddot{\boldsymbol{u}}_{DCB,modal} + \boldsymbol{K}_{DCB,modal}\boldsymbol{u}_{DCB,modal} = \boldsymbol{T}_{DCB,modal}^T \bar{\boldsymbol{f}}_{DCB} \tag{14.46}$$

with

$$\boldsymbol{M}_{DCB,modal} = \boldsymbol{T}_{DCB,modal}^T \bar{\boldsymbol{M}}_{DCB} \boldsymbol{T}_{DCB,modal} = \boldsymbol{T}_{DCB,modal}^T \bar{\boldsymbol{T}}_{DCB}^T \boldsymbol{M}_{dual} \bar{\boldsymbol{T}}_{DCB} \boldsymbol{T}_{DCB,modal} \,, \tag{14.47}$$

$$\boldsymbol{K}_{DCB,modal} = \boldsymbol{T}_{DCB,modal}^T \bar{\boldsymbol{K}}_{DCB} \boldsymbol{T}_{DCB,modal} = \boldsymbol{T}_{DCB,modal}^T \bar{\boldsymbol{T}}_{DCB}^T \boldsymbol{K}_{dual} \bar{\boldsymbol{T}}_{DCB} \boldsymbol{T}_{DCB,modal} \,, \tag{14.48}$$

$$\boldsymbol{u}_{DCB,modal} = \begin{bmatrix} \boldsymbol{\eta} \\ \tilde{\boldsymbol{\lambda}} \end{bmatrix}, \qquad \boldsymbol{f}_{DCB,modal} = \boldsymbol{T}_{DCB,modal}^T \bar{\boldsymbol{f}}_{DCB} = \boldsymbol{T}_{DCB,modal}^T \bar{\boldsymbol{T}}_{DCB}^T \boldsymbol{f}_{dual} \,. \tag{14.49}$$

Eq. (14.46) can be written as

$$\begin{bmatrix} \boldsymbol{I} & -\boldsymbol{\Omega}^{-2} \boldsymbol{\Theta}^T \boldsymbol{B}^T \boldsymbol{X}_\lambda \\ -\boldsymbol{X}_\lambda^T \boldsymbol{B} \boldsymbol{\Theta} \boldsymbol{\Omega}^{-2} & \boldsymbol{I} \end{bmatrix} \begin{bmatrix} \ddot{\boldsymbol{\eta}} \\ \ddot{\tilde{\boldsymbol{\lambda}}} \end{bmatrix} + \begin{bmatrix} \boldsymbol{\Omega}^2 & \boldsymbol{0} \\ \boldsymbol{0} & \boldsymbol{\mu}^2 \end{bmatrix} \begin{bmatrix} \boldsymbol{\eta} \\ \tilde{\boldsymbol{\lambda}} \end{bmatrix} = \boldsymbol{T}_{DCB,modal}^T \bar{\boldsymbol{T}}_{DCB}^T \boldsymbol{f}_{dual} \tag{14.50}$$

which shows the relation between generalized modal parameters of the substructures $\boldsymbol{\eta}$ and the generalized interface parameters $\tilde{\boldsymbol{\lambda}}$. The physical displacement $\boldsymbol{u}$ of the original system can be reconstructed by the simple back transformation

$$\begin{bmatrix} \boldsymbol{u} \\ \boldsymbol{\lambda} \end{bmatrix} = \bar{\boldsymbol{T}}_{DCB} \boldsymbol{T}_{DCB,modal} \begin{bmatrix} \boldsymbol{\eta} \\ \tilde{\boldsymbol{\lambda}} \end{bmatrix} = \begin{bmatrix} \boldsymbol{\Theta} & (\boldsymbol{R}\boldsymbol{X}_\alpha - \boldsymbol{G}\boldsymbol{B}^T \boldsymbol{X}_\lambda) \\ \boldsymbol{0} & \boldsymbol{X}_\lambda \end{bmatrix} \begin{bmatrix} \boldsymbol{\eta} \\ \tilde{\boldsymbol{\lambda}} \end{bmatrix} \tag{14.51}$$

The size of the DCBM reduced system with modal interface reduction is $n_{DCB,modal} = \sum_{s=1}^{N} n_\theta^{(s)} + n_x$. If, as described before, the alternative formulation of the DCBM using attachment modes is applied the dual interface modes do not change no matter how many free interface vibration modes are included in the reduction basis. The corresponding eigenvalue problem (14.41) does not change and therefore the interface reduction can be conducted first and afterwards the reduction basis can be enriched by an arbitrary number of free interface vibration modes without affecting Eq. (14.41).

14.4 Numerical Example of Two-Dimensional Solid

In order to demonstrate the approximation accuracy of the DCBM with interface reduction, as described in Sect. 14.3, the problem of a two dimensional rectangle decomposed in 12 substructures as illustrated in Fig. 14.1 is considered [7]. Each substructure is discretized by 16×9 bilinear four-noded elements (plane stress) and the structure is clamped on the left side in both directions. This gives 4020 DOFs in the displacement vector $\boldsymbol{u}$ and $n_\lambda = 436$ Lagrange multipliers resulting in a total number of $n_{total} = 4456$ DOFs of Eq. (14.7). The objective is to approximate the lowest eigenfrequencies ω of the full structure with the DCBM and with the DCBM with additional interface reduction. Using 8 free interface normal modes per substructure (not including potential rigid body modes) the relative error

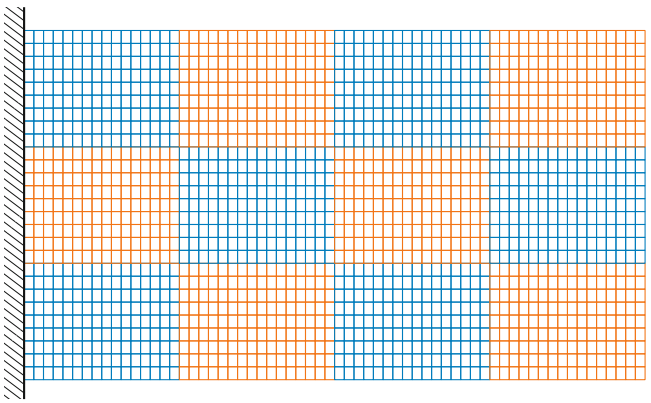

Fig. 14.1 Two dimensional solid problem decomposed in 12 substructures. Each substructure is discretized by 16×9 bilinear four-noded elements (plane stress) and the structure is clamped on the left side in both directions [7]

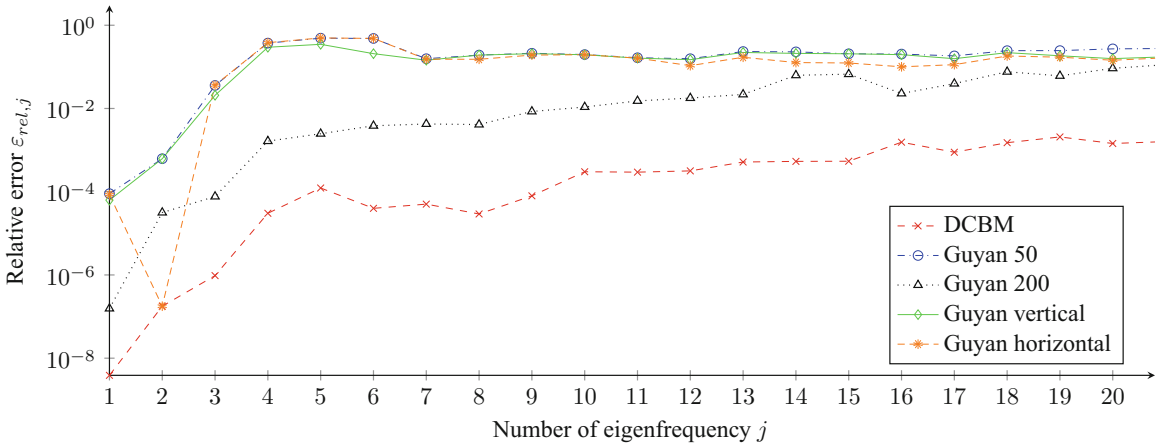

Fig. 14.2 Relative error of DCBM and DCBM with Guyan interface reduction

Table 14.1 Excerpt of eigenvalues after DCBM reduction without interface reduction. The first negative eigenvalue is the 82nd value

j	Eigenvalue
80	2.303
81	2.324
82	−2.360
83	−2.361
84	2.398

$$\varepsilon_{rel,j} = \frac{|\omega_{red,j} - \omega_{full,j}|}{\omega_{full,j}} \tag{14.52}$$

of eigenfrequency j depicted in Fig. 14.2 is resulting (graph denoted by "DCBM") with $\omega_{red,j}$ being the j-th eigenfrequency of the reduced system and $\omega_{full,j}$ being the j-th eigenfrequency of the full (non-reduced) system, which is computed additionally. The eigenfrequencies are ordered by ascending values. In this example the DCBM reduces the total number of $n_{total} = 4456$ DOFs to $n_{DCB} = n_{rig} + n_\theta + n_\lambda = 27 + 96 + 436 = 559$ DOFs (which is a reduction of around 88% of the number of degrees of freedom). But this makes also the necessity of an interface reduction obvious since in this example the number of Lagrange multipliers $n_\lambda = 436$, which has a significant contribution to the number of DOFs of the DCBM reduced system, remains unchanged. The number of Lagrange multipliers $n_\lambda = 436$ still make around 78% of the degrees of freedom of the DCBM reduced system. This makes an interface reduction absolutely essential which is demonstrated in the following by way of example. Note that the first negative eigenvalue is the 82nd in the case of DCBM without interface reduction as illustrated in Table 14.1.

14.4.1 Guyan Reduction of Interface Coordinates

To illustrate the DCBM with Guyan interface reduction we reduce the number of rigid body modes and Lagrange multipliers of $n_{rig} + n_\lambda = 27 + 436 = 463$ to $n_{kept} = 200$ kept DOFs. As criterion for the choice of the kept DOFs the quotient K_{ii}/M_{ii} of the diagonal entries of the stiffness and mass matrix is used. Giving zero for rigid body modes all these modes are kept. The size of the reduced system is now $n_{Guyan} = 96 + 200 = 296$ and the corresponding graph showing the relative error of this reduction in Fig. 14.2 is denoted by "Guyan 200". The reduced system has a number of negative eigenvalues equal to the number of kept Lagrange multipliers $n_{\lambda,k} = 173$. The approximation accuracy of the eigenvalues compared to the DCBM without interface reduction is decreased by a factor around 100. The first negative eigenvalue of the system with Guyan interface reduction is the 117th eigenvalue, as shown in Table 14.2. Compared to the DCBM without interface reduction (82th eigenvalue is the first negative, see Table 14.1), negative eigenvalues occur now in the a higher frequency spectrum which can have some advantages. Note that the computational effort of the Guyan reduction is very small compared to a modal interface reduction since no additional eigenvalue problem has to be solved.

Table 14.2 Excerpt of eigenvalues after DCBM reduction with Guyan interface reduction ($n_{int} = 200$ interface modes kept). The first negative eigenvalue is the 117rd value

j	Eigenvalue
115	2.341
116	2.395
117	−2.427
118	2.563
119	2.617

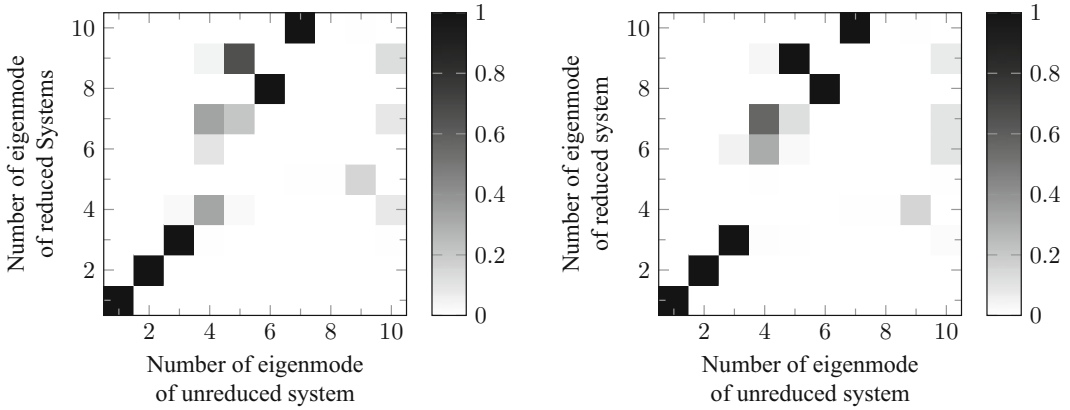

Fig. 14.3 MAC for DCBM reduced system with Guyan interface reduction. (**a**) DCBM with Guyan interface reduction (vertical DOFs kept). (**b**) DCBM with Guyan interface reduction (horizontal DOFs kept)

If the number of rigid body modes an Lagrange multipliers is reduced to only $n_{Guyan} = 50$ DOFs, the results become considerably worse which is shown by the graph "Guyan 50" in Fig. 14.2. Already the 4th eigenfrequency has an error greater than 10% which is an amount not acceptable in practical applications.

Analogous to Guyan interface reduction for the Craig-Bampton method [3], in which the displacement DOFs of the interface can be divided into horizontal and vertical DOFs, the Lagrange multipliers can divided in the same way. In the following a Guyan interface reduction is performed the one time keeping rigid body modes and vertical Lagrange multipliers and the other times keeping rigid body modes and horizontal Lagrange multipliers as reduced interface DOFs. The results for both computations are shown in Fig. 14.2 and denoted by "Guyan vertical" and "Guyan horizontal", respectively. Except the 2nd eigenfrequency the two graphs are almost parallel. Figure 14.3a, b show the MAC (modal assurance criterion) values of the two Guyan interface reductions when comparing the modes of the unreduced system to the modes of the DCBM reduced system with Guyan interface reduction, respectively. Both figures are hardly different and therefore, compared to the Guyan interface reduction for the Craig-Bampton method [3], it can not be concluded anymore that retaining vertical interface DOFs improves the approximation of eigenmodes with mainly vertical direction of movement or that retaining horizontal interface DOFs improves the approximation of eigenmodes with mainly horizontal direction of movement significantly. This effect is only visible for the 2nd eigenmode which is the 1st longitudinal mode and is represented by the horizontal Lagrange multipliers with high accuracy. The reason is that rigid body modes are retained for DCBM with Guyan reduction in any case. The rigid body modes have contributions in vertical and horizontal direction such that eigenmodes with displacements in both directions can be approximated in a certain accuracy range even if only Lagrange multipliers in one direction are kept. Nevertheless the approximation accuracy is poor for both cases considering the relative errors in Fig. 14.2 and the correlations of the MAC values in Fig. 14.3.

14.4.2 Modal Reduction of Interface Coordinates

For the demonstration of the DCBM with modal reduction of interface coordinates again the system depicted in Fig. 14.1 is considered. As described at the beginning of Sect. 14.4, the DCBM reduction gives a reduced system with $n_{DCB} = n_{rig} + n_\theta + n_\lambda = 27 + 96 + 436 = 559$ remaining DOFs for this example. $n_\theta = 12 \cdot 8 = 96$ is the number of kept free interface normal modes of all twelve substructures, $n_{rig} = 9 \cdot 3 = 27$ the number of rigid body modes of all (free floating) substructures and $n_\lambda = 436$ the number of Lagrange multipliers. Therefore the system has 123 positive and 436 negative

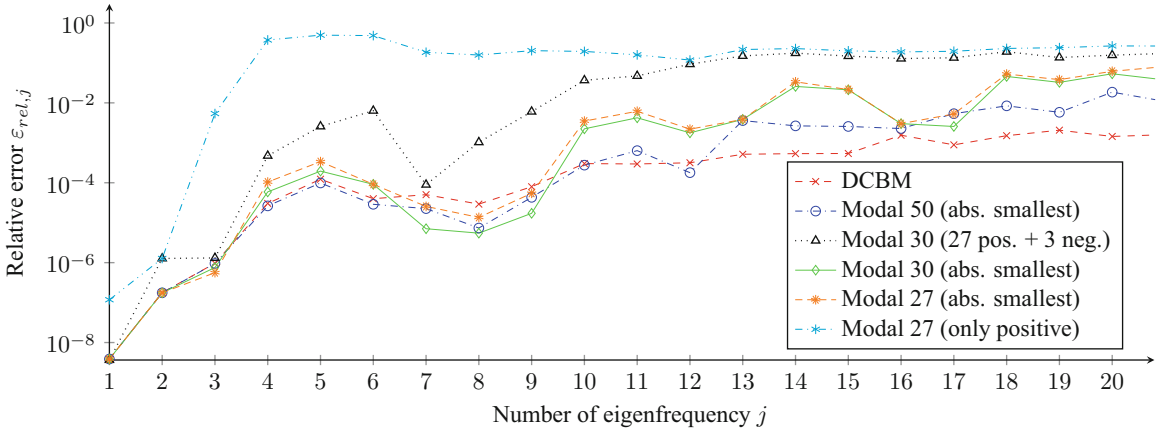

Fig. 14.4 Relative error of DCBM and DCBM with modal interface reduction

Table 14.3 First eigenvalues of dual interface problem

j	Eigenvalue
1	0.0009
2	0.0097
3	0.0132
4	−0.0228
5	−0.0234
6	−0.0264
7	0.0647
8	0.0917
9	0.0933
10	0.0991

eigenvalues corresponding to the kept free interface normal modes (including the rigid body modes) and the Lagrange multipliers, respectively [6]. The relative error of the eigenfrequencies of the reduced system in the low frequency range using 8 free interface normal modes per substructure are depicted in Fig. 14.4 (graph is denoted by "DCBM") and will be used as reference for the modal interface reduction with different numbers of kept interface modes in the following [6].

14.4.2.1 Modal Interface Reduction with 50 Interface Modes

Now the rigid body modes and the Lagrange multipliers are reduced to $n_{int} = 50$ interface DOFs resulting in a reduced system of size $n_{DCB,Modal} = 146$. Table 14.3 illustrates that already in the low frequency range interface modes with corresponding negative eigenvalues occur. As criterion for the choice of the kept interface modes, the lowest absolute eigenvalue is used. The interface problem has 27 interface modes with positive eigenvalues corresponding to the number of rigid body modes and 436 interface modes with negative eigenvalues corresponding to the number of Lagrange multipliers, respectively. Among the $n_{int} = 50$ kept interface modes with lowest absolute eigenvalues are 26 interface modes with positive eigenvalues and 24 interface modes with negative eigenvalues. Keeping 24 interface modes with negative eigenvalues, the reduced system has 24 negative eigenvalues as well. The graph denoted by "Modal 50" in Fig. 14.4 depicts the relative errors of the lowest eigenfrequencies of this interface reduction.

The relative error of the first four eigenfrequencies is approximated as good as for the DCBM without interface reduction (graph "DCBM"). Surprisingly, the relative errors with interface reduction of the subsequent eigenfrequencies are lower up to the 10th eigenfrequency. A few values are thus approximated better with interface reduction than without interface reduction. This is not intuitive since errors are expected to be lower when no interface reduction is carried out. However since the DCBM is reducing a problem written in primal and dual variables the convergence is not guaranteed to be monotonic [11]. It is also noteworthy that the negative eigenvalues after modal interface reduction take the greatest absolute values of all eigenvalues. That means, if the eigenvalues are sorted by absolute values, the negative values are at the upper end of the spectrum. All 122 positive eigenvalues have smaller absolute values than the 24 negative eigenvalues. Against that, the first negative eigenvalue is the 82nd in the case of applying the DCBM without interface reduction. As the case here, it is often advantageous negative

Table 14.4 Excerpt of eigenvalues after DCBM reduction with modal interface reduction ($n_{int} = 50$ interface modes kept). The first negative eigenvalue is the 123rd value

j	Eigenvalue
120	3.238
121	3.412
122	3.535
123	−4.923
124	−5.989

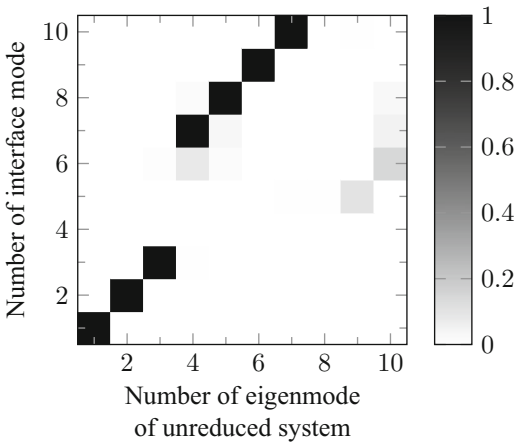

Fig. 14.5 MAC for dual interface modes

eigenvalues only appearing in the higher frequency range. Tables 14.1 and 14.4 show excerpts from the eigenvalue spectrum in which the first negative eigenvalues appear. Since eigenmodes with negative eigenvalues are non-physical and, for instance, can lead to problems during time integration, it is obvious to prefer interface modes with positive eigenvalues and not only take the absolute values of the eigenvalues as criterion for the choice of the kept interface modes.

14.4.2.2 Modal Interface Reduction with 30 Interface Modes

Keeping $n_{int} = 50$ interface modes corresponding to the eigenvalues with smallest absolute values in the previous example (Sect. 14.4.2.1) led to 24 interface modes with negative eigenvalues and 26 with positive eigenvalues. If we were taken now all 27 interface modes with positive eigenvalues and fill up with 23 interface modes with negative eigenvalues with smallest absolute value (keeping the number of interface modes $n_{int} = 50$ constant) the basis for the interface modes would only change by one mode.

Therefore we consider now the case only keeping the $n_{int} = 30$ interface modes for the modal interface reduction. On the one hand we keep the interface modes with smallest absolute values leading to kept interface modes corresponding to 17 positive and 13 negative eigenvalues. On the other hand we keep all 27 interface modes with positive eigenvalues and fill up with only 3 interface modes with negative eigenvalues to obtain a interface reduction basis of dimension $n_{int} = 30$. Figure 14.4 depicts the relative errors of the lowest 20 eigenfrequencies for the two cases denoted by "Modal 30 (27 pos. + 3 neg.)" and "Modal 30 (abs. smallest)", respectively.

The approximation of the eigenfrequencies is much better for the interface modes corresponding to the smallest absolute values (graph "Modal 30 (abs. smallest)" in Fig. 14.4). For the first three eigenfrequencies the relative errors are comparable to the error of the DCBM without interface reduction. Starting from the 4th eigenfrequency the modal interface reduction with the interface modes corresponding to the 30 smallest absolute values is around one order better than the reduction keeping all interface modes corresponding to positive eigenvalues in the reduction basis.

It can be concluded that for the most accurate approximation of the eigenfrequencies of the system applying modal interface reduction, the interface modes corresponding to negative eigenvalues have significant contributions. The interface modes corresponding to negative eigenvalues are necessary for the most accurate calculation of the eigenfrequencies. It is recommended to keep the interface modes for the modal interface reduction with corresponding smallest absolute eigenvalues which is not intuitive.

Figure 14.5 shows the MAC numbers for the first 10 global eigenmodes of the unreduced system and the first 10 dual interface modes. Figure 14.6 shows the first and fourth dual interface mode of the system. The interface mode corresponding to a negative eigenvalues in Fig. 14.6b shows large interface incompatibility which makes it for the time being difficult to imagine that this mode improves the approximation accuracy.

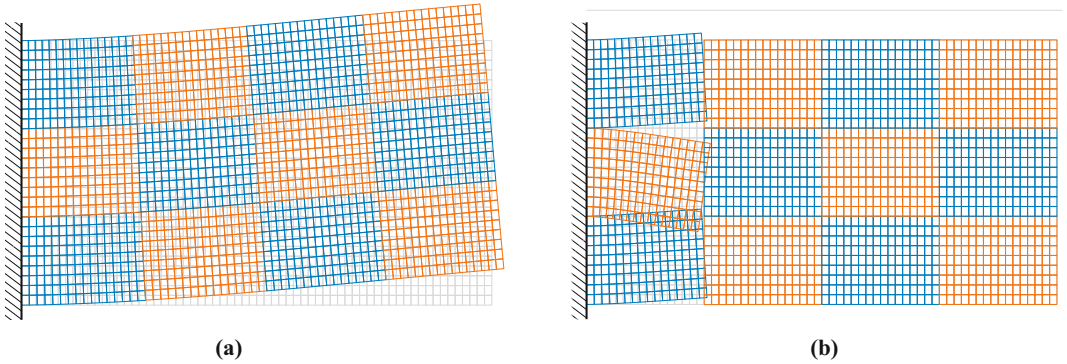

(a) **(b)**

Fig. 14.6 Dual interface modes of wo dimensional solid problem decomposed in 12 substructures (see Fig. 14.1). (**a**) First interface mode. (**b**) Fourth interface mode

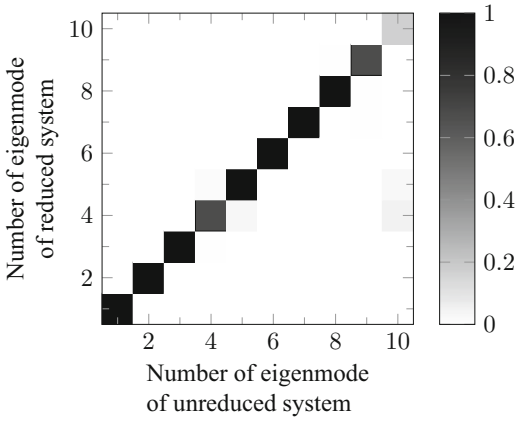

Fig. 14.7 MAC for DCBM reduced system with modal interface reduction ($n_{int} = 27$ interface modes with positive eigenvalues kept)

The dual interface modes with negative eigenvalues (number 4, 5 and 6) do not have any correlation to the first eigenmodes of the unreduced system. All other interface modes correlate strongly to eigenmodes of the unreduced system. Nevertheless the graphs in Fig. 14.4 indicate clearly that the interface modes corresponding to negative eigenvalues improve the approximation accuracy while keeping the final size of the reduced system constant.

14.4.2.3 Modal Interface Reduction with 27 Interface Modes

Since in many applications, for example time integration, negative eigenvalues cause major problems, now a modal interface reduction is investigated which uses only all the 27 interface modes with positive eigenvalues. Therefore the reduced system does not have an negative eigenvalues anymore. In this example the system is reduced to size $n_{DCB,Modal} = 96 + 27 = 123$. For comparison a second interface reduction is conducted which keeps 27 interface modes corresponding to the eigenvalues with smallest absolute values. The graphs "Modal 27 (only positive)" and "Modal 27 (abs. smallest)" in Fig. 14.4 show the relative errors for these two computations.

The approximation accuracy for the interface reduction with interface modes corresponding to only positive eigenvalues is acceptable for the first 3 eigenfrequencies. From the 4th eigenfrequency the relative error is already over 10% which is a very poor approximation. In contrast to this, the accuracy of modal interface reduction with interface modes corresponding to the smallest absolute eigenvalues is significantly better for all of the first 20 eigenfrequencies. This emphasizes the positive effect of the interface modes corresponding to negative eigenvalues on the approximation accuracy of the lowest eigenfrequencies of the system.

Considering the MAC numbers for the first 10 global eigenmodes of the unreduced system and the first 10 eigenmodes of the reduced system with interface reduction using only the interface modes corresponding to the 27 positive eigenvalues in Fig. 14.7, it is noteworthy that the MAC number is greater than 0.8 up to the 8th eigenvalue. This shows that the eigenmodes of the reduced system are approximating the eigenmodes of the unreduced system very good although the eigenfrequencies of these modes show large errors (more than 10%) starting with the 4th eigenfrequency (see Fig. 14.4). It can be concluded that keeping the interface modes corresponding to positive eigenvalues results in a good approximation of the eigenmodes of the unreduced system but the corresponding eigenfrequencies are not approximated so well.

14.4.3 Interpretation of Dual Interface Normal Modes

In this section all computations refer to the system depicted in Fig. 14.8 which is a simplification of the system in Fig. 14.1 and is used now for the sake of simplicity. This gives 660 DOFs in the displacement vector $\boldsymbol{u}$ and $n_\lambda = 20$ Lagrange multipliers resulting in a total size of the dual assembled system of 680. The shapes of the eigenmodes of the unreduced system of Fig. 14.8 corresponding to the 8 lowest eigenfrequencies are shown in Fig. 14.9. The 1st eigenmode represents the 1st bending mode with vibration node at the clamped end. The 2nd eigenmode corresponds to the 1st longitudinal mode having the vibration node also at the clamped end. The 3rd, 4th, 6th, 7th and 8th eigenmode represents the 2nd, 3rd, 4th, 5th and 6th bending mode, respectively, while the 5th eigenmode represents the 2nd longitudinal mode.

For the time being the system is reduced by the DCBM using 8 free interface normal modes per substructure and additionally 3 rigid body modes for the right substructure which is free floating. The original system of size $n_{total} = 680$ is reduced by the DCBM to $n_{DCB} = n_\theta + n_{rig} + n_\lambda = 39$ remaining DOFs with the number of free interface normal modes $n_\theta = 2 \cdot 8 = 16$, the number of rigid body modes $n_{rig} = 3$ and the number of Lagrange multipliers $n_\lambda = 20$. This reduced system is the starting point for the analysis of the modal interface reduction of the DCBM. In the following the number of kept free interface modes is varied systematically to gain insight into the interface reduction method.

First of all we want to consider the first 5 dual interface modes corresponding to the smallest absolute eigenvalues in Fig. 14.10. There are 23 interface modes in total. Three of them have positive corresponding eigenvalues (according to the number of the rigid body modes) and 20 of them have negative eigenvalues (according to the number of Lagrange

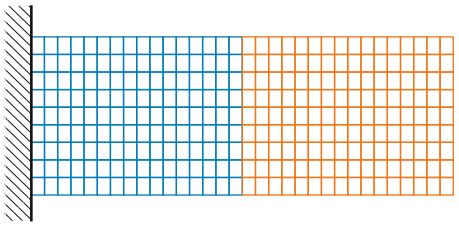

Fig. 14.8 Two dimensional solid problem decomposed in two substructures

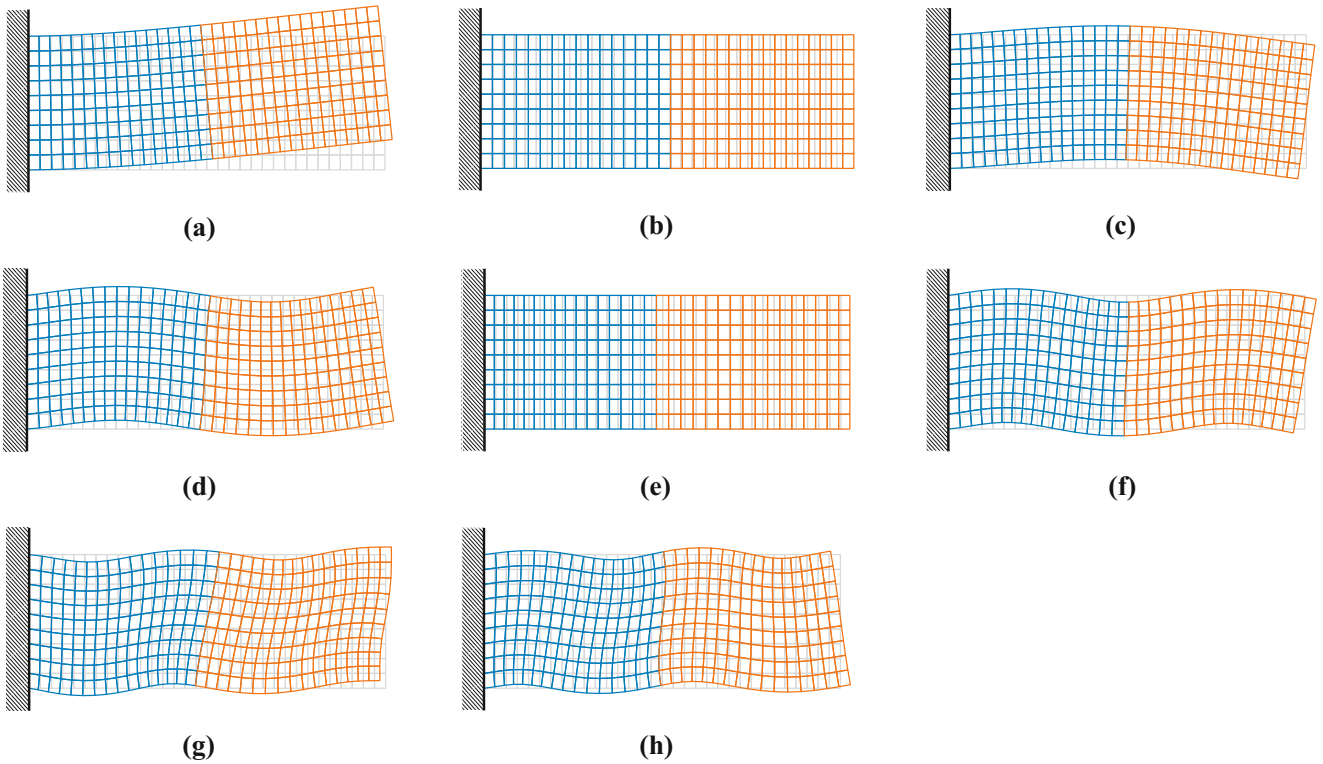

Fig. 14.9 First eight eigenmodes of the system depicted in Fig. 14.8 (without any reduction). (**a**) 1. eigenmode: $\omega^2 = 0.0019$. (**b**) 2. eigenmode: $\omega^2 = 0.0386$. (**c**) 3. eigenmode: $\omega^2 = 0.0398$. (**d**) 4. eigenmode: $\omega^2 = 0.1911$. (**e**) 5. eigenmode: $\omega^2 = 0.3476$. (**f**) 6. eigenmode: $\omega^2 = 0.4409$. (**g**) 7. eigenmode: $\omega^2 = 0.7229$. (**h**) 8. eigenmode: $\omega^2 = 0.8441$

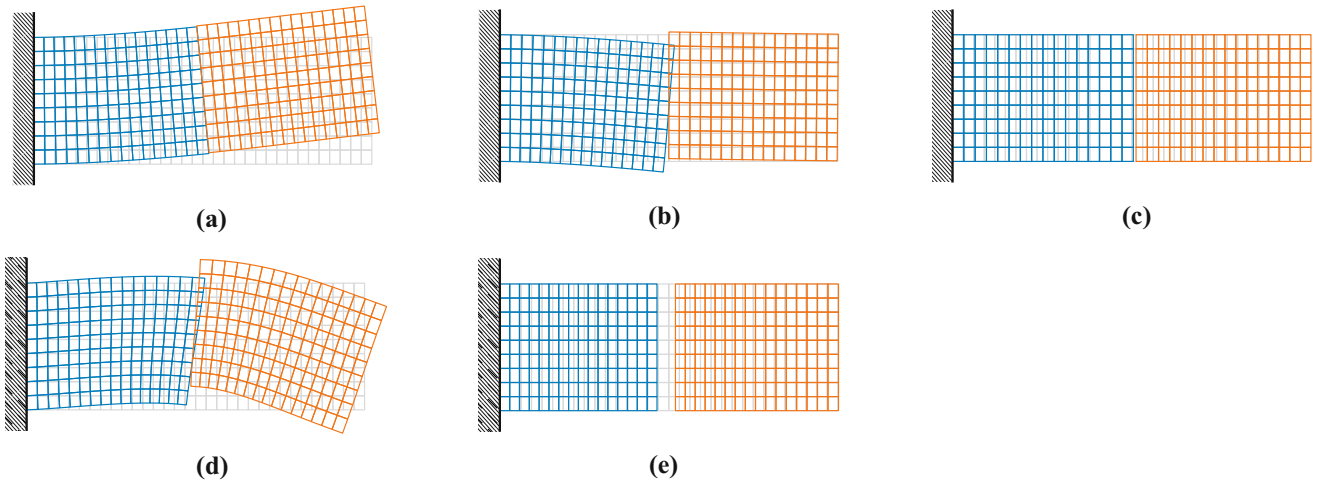

Fig. 14.10 First five dual interface modes. (**a**) 1. interface mode: $\omega^2 = 0.0019$. (**b**) 2. interface mode: $\omega^2 = -0.0298$. (**c**) 3. interface mode: $\omega^2 = 0.0400$. (**d**) 4. interface mode: $\omega^2 = 0.0565$. (**e**) 5. interface mode: $\omega^2 = -0.2744$

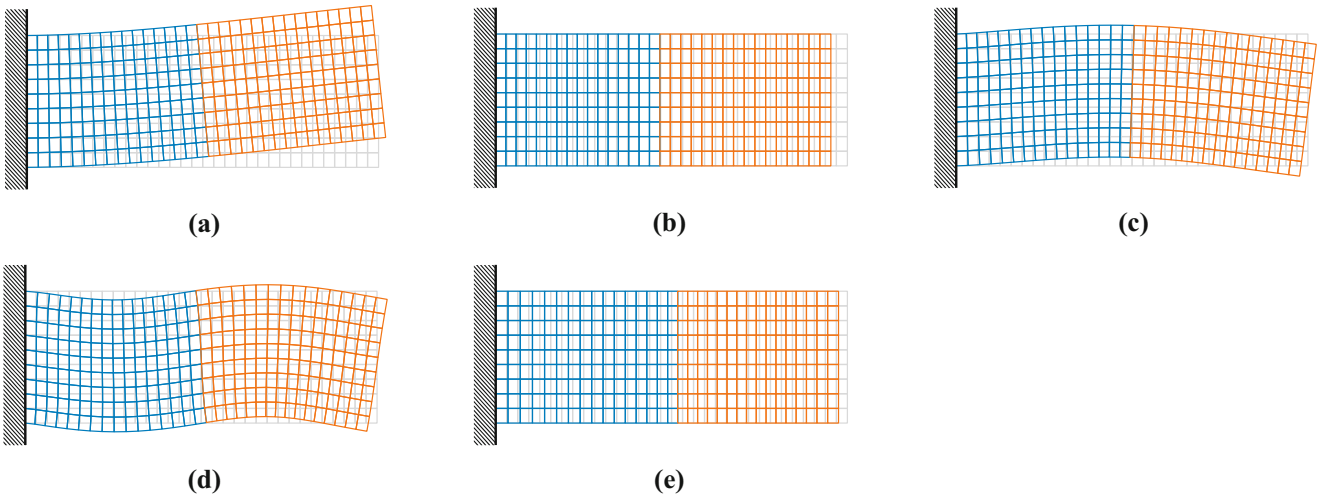

Fig. 14.11 First five eigenmodes after DCBM ($n_\theta^{(1)} = n_\theta^{(2)} = 8$) without interface reduction. (**a**) 1. eigenmode: $\omega^2_{DCB} = 0.0019$. (**b**) 2. eigenmode: $\omega^2_{DCB} = 0.0386$. (**c**) 3. eigenmode: $\omega^2_{DCB} = 0.0398$. (**d**) 4. eigenmode: $\omega^2_{DCB} = 0.1912$. (**d**) 5. eigenmode: $\omega^2_{DCB} = 0.3479$

multipliers). The 3 interface modes corresponding to the positive eigenvalues seem to be physically meaningful since the 1st and 4th mode in Fig. 14.10 look like the first 2 bending modes of the unreduced system in Fig. 14.1 and the 3rd interface modes looks similar to the 1st longitudinal mode of the unreduced system. Because of the high interface incompatibilities of the interface modes corresponding to negative eigenvalues no comparable equivalent can be found for these modes.

14.4.3.1 Dual Craig-Bampton Reduction Without Interface Reduction

First of all, the system of Fig. 14.8 is reduced by the DCBM using 8 free interface normal modes per substructure from $n_{total} = 680$ DOFs to $n_{DCB} = 39$ DOFs. The shapes of the eigenmodes corresponding to the 5 smallest absolute eigenvalues of the reduced system are shown in Fig. 14.11. The first eigenmodes of the reduced system (Fig. 14.11) show a high correlation to the eigenmodes of the unreduced system (Fig. 14.8) which is also confirmed by the MAC values of the first 10 eigenmodes in Fig. 14.14a. The relative error of the eigenfrequencies of the reduced system in the low frequency range using 8 free interface normal modes per substructure without interface reduction are depicted in Fig. 14.12 (graph is denoted by "DCBM") and will be used as reference for the modal interface reduction in the following.

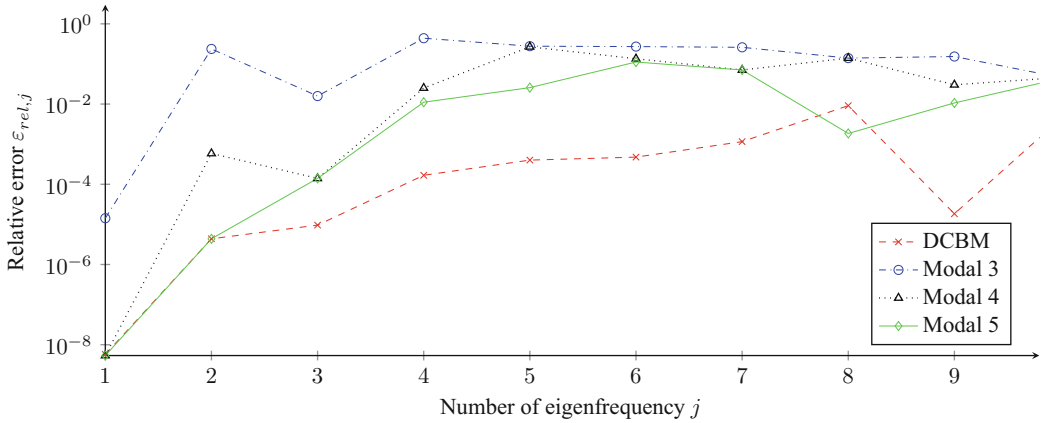

Fig. 14.12 Relative error of DCBM and DCBM with modal interface reduction with 3, 4 or 5 kept interface modes

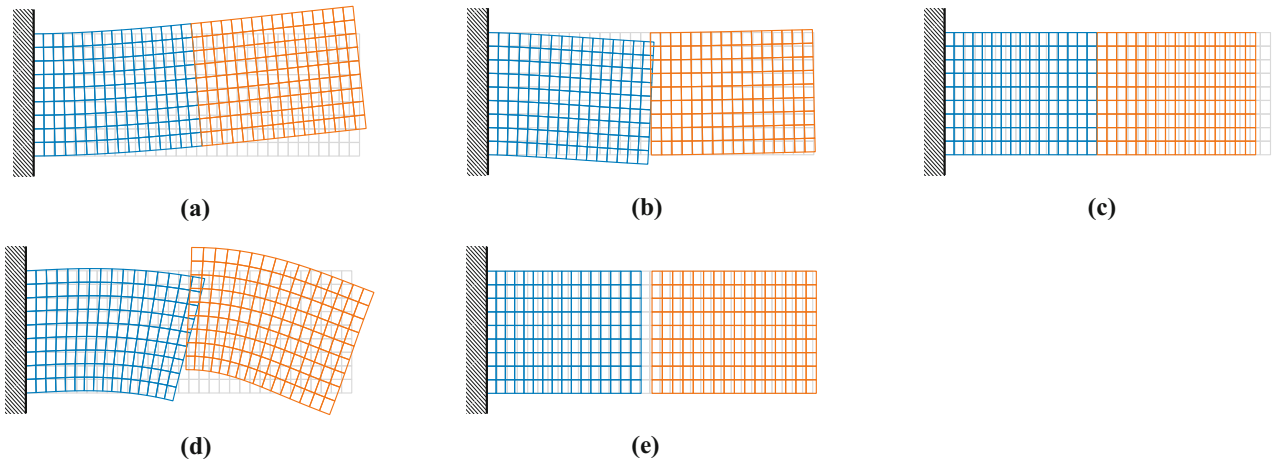

Fig. 14.13 First five eigenmodes after DCBM ($n_\theta^{(1)} = n_\theta^{(2)} = 8$) with modal interface reduction ($n_{int} = 3$ interface modes kept). (**a**) 1. eigenmode: $\omega^2_{DCB,mod} = 0.0019$. (**b**) 2. eigenmode: $\omega^2_{DCB,mod} = 0.0225$. (**c**) 3. eigenmode: $\omega^2_{DCB,mod} = 0.0385$. (**d**) 4. eigenmode: $\omega^2_{DCB,mod} = 0.0603$. (**e**) 5. eigenmode: $\omega^2_{DCB,mod} = 0.1816$

14.4.3.2 Modal Interface Reduction with Three Interface Modes Corresponding to the Three Positive Eigenvalues

For the investigation of the modal interface reduction exclusively the 3 interface modes corresponding to positive eigenvalues are used first. This leads to a reduced system without negative eigenvalues. The graph "Modal 3" in Fig. 14.12 shows the relative errors of the eigenfrequencies with this interface reduction. Only the first eigenfrequency is approximated with acceptable accuracy. From the second eigenfrequency the relative errors are at least 10% which is unacceptable at the first glance.

Considering the shapes of the eigenmodes of the reduced system in Fig. 14.13 and the MAC values in Fig. 14.14b leads to the insight that the graph in Fig. 14.12 has to be looked at differently. Figure 14.13a shows that there is a high correlation between the 1st bending mode of the reduced system (Fig. 14.13a) and the 1st bending mode of the unreduced system (Fig. 14.9a). Moreover the 3rd eigenmodes of the reduced system (Fig. 14.13c) correlates highly with the 2nd eigenmode of the unreduced system (Fig. 14.9b), which is also confirmed by a MAC value near 1 as shown in Fig. 14.14b.

In addition the relative error between the corresponding eigenvalues of these two modes is very low. Though a mode with high interface incompatibility shows up at 2nd position after the interface reduction (see Fig. 14.13b) which looks similar to the interface mode corresponding to the negative eigenvalue with smallest absolute value as shown in Fig. 14.10b. Hence eigenfrequencies of modes, which do not correlate, are compared in the calculation of the relative errors according to Eq. (14.52). As shown in Fig. 14.14b there is no high correlation between the first 10 eigenmodes of the reduced and the unreduced system. The interface incompatibilities of the 4th and 5th eigenmodes are also very high (Fig. 14.13d, e). Therefore we want demonstrate the effect adding more interface modes for this example in the following.

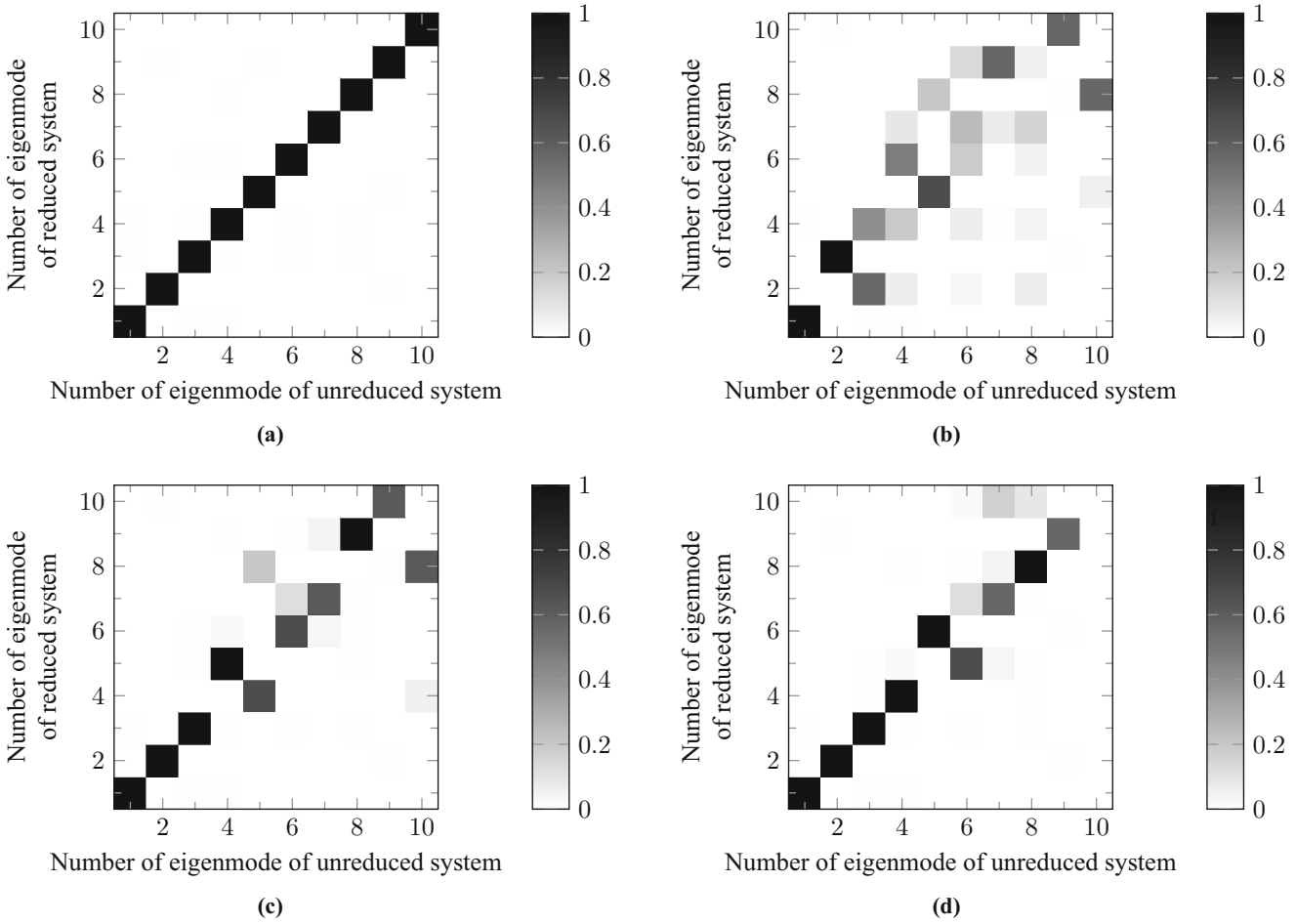

Fig. 14.14 MAC for DCBM reduced system with and without modal interface reduction. (**a**) DCBM. (**b**) DCBM with $n_{int} = 3$ kept interface modes. (**c**) DCBM with $n_{int} = 4$ kept interface modes. (**d**) DCBM with $n_{int} = 5$ kept interface modes

14.4.3.3 Modal Interface Reduction with Three Interface Modes Corresponding to the Three Positive Eigenvalues Plus One Additional Interface Mode Corresponding to the Negative Eigenvalue with Smallest Absolute Value

For further investigation a modal interface reduction is conducted again, but the interface mode corresponding to the negative eigenvalues with smallest absolute values (mode shape shown in Fig. 14.10b) is added to the 3 interface modes corresponding to the positive eigenvalues as demonstrated in Sect. 14.4.3.2. The graph "Modal 4" in Fig. 14.12 shows the relative errors of the first 10 eigenfrequencies with this interface reduction. Including the 2nd interface mode enhances the approximation significantly, especially the relative errors of the first 4 eigenfrequencies are improved noticeably. Figure 14.15 depicts the mode shapes corresponding to the 8 lowest eigenvalues of the reduced system and the MAC values of the first 10 eigenmodes between the unreduced and reduced system are shown in Fig. 14.14c. Figure 14.15a–c demonstrate that the first 3 eigenmodes of the unreduced system are represented very accurate by the reduced system with 4 kept interface modes. This is confirmed by MAC values near 1 in Fig. 14.14c. Moreover the eigenvalue errors for these modes are very small and only very low interface incompatibilities can be seen.

The 2nd (incompatible) eigenmode of the previous section (Fig. 14.13b) seems to be compensated by including the interface mode corresponding to the smallest negative eigenvalue (Fig. 14.10b) in such a way that the first 3 eigenmodes show up in the right order now. Moreover the MAC values in Fig. 14.14c illustrate that the 5th eigenmode of the reduced system (Fig. 14.13e) correlates to the 4th eigenmode of the unreduced system (Fig. 14.9d). The difference between the corresponding eigenvalues is also very small.

But one mode with high interface incompatibility shows up at 4th position in Fig. 14.15. This modes seems to correlate to the 5th eigenmode, which is the 2nd longitudinal mode, of the unreduced system as indicated by the corresponding MAC

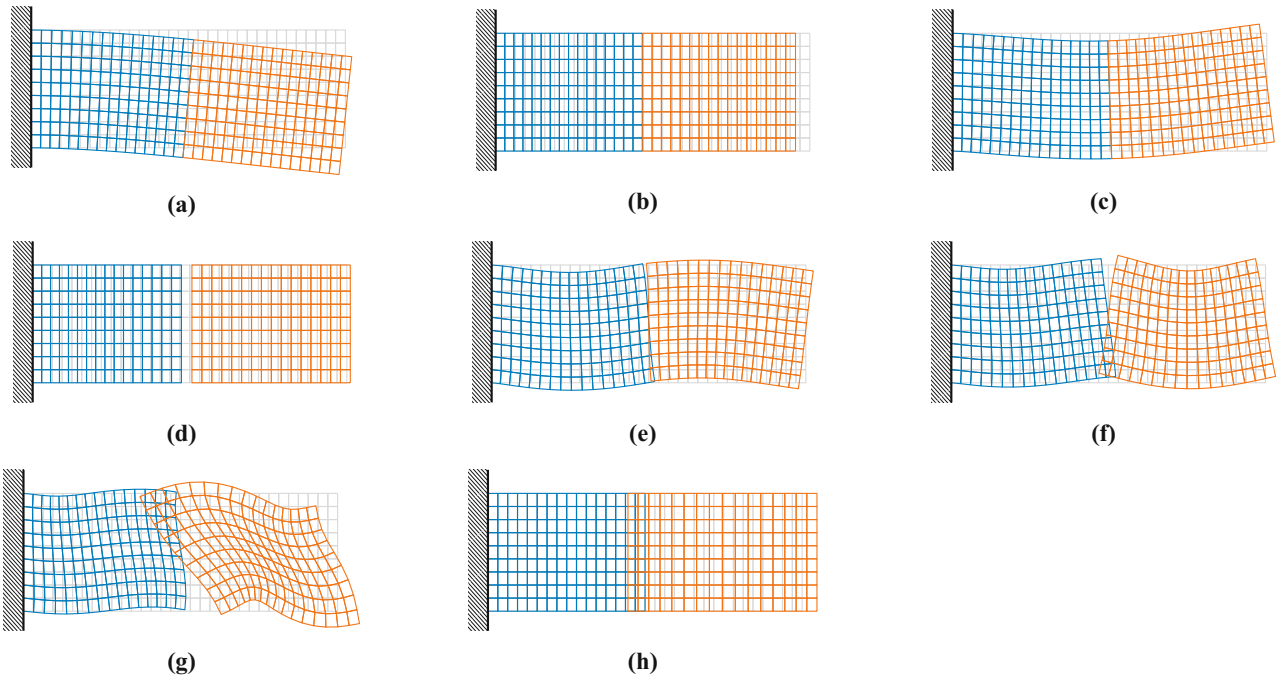

Fig. 14.15 First eight eigenmodes after DCBM ($n_\theta^{(1)} = n_\theta^{(2)} = 8$) with modal interface reduction ($n_{int} = 4$ interface modes kept). (**a**) 1. eigenmode: $\omega^2_{DCB,mod} = 0.0019$. (**b**) 2. eigenmode: $\omega^2_{DCB,mod} = 0.0385$. (**c**) 3. eigenmode: $\omega^2_{DCB,mod} = 0.0398$. (**d**) 4. eigenmode: $\omega^2_{DCB,mod} = 0.1816$. (**e**) 5. eigenmode: $\omega^2_{DCB,mod} = 0.1869$. (**f**) 6. eigenmode: $\omega^2_{DCB,mod} = 0.3300$. (**g**) 7. eigenmode: $\omega^2_{DCB,mod} = 0.6243$. (**h**) 8. eigenmode: $\omega^2_{DCB,mod} = 0.6247$

value in Fig. 14.14c. The 6th and 7th mode of the reduced system correlate to the respective modes of the unreduced system according to the MAC values but there are high incompatibilities in the mode shapes depicted in Fig. 14.15f, g.

To sum up, it can be concluded that including the interface modes corresponding to negative eigenvalues improves the approximation accuracy significantly which will be refined in the subsequent section. Especially the first 3 bending modes of the system can be represented much better in this example and also the interface incompatibilities are reduced significantly. That is not the case without including this additional interface mode.

14.4.3.4 Modal Interface Reduction with Three Interface Modes Corresponding to the Three Positive Eigenvalues Plus Two Additional Interface Mode Corresponding to the Two Negative Eigenvalues with Smallest Absolute Values

Finally one more additional interface mode corresponding to a negative eigenvalue is added to the reduction basis. This interface mode has also strong interface incompatibilities as depicted in Fig. 14.10e. In total 5 interface modes are used now whereby 3 of them have positive eigenvalues and the other 2 have negative eigenvalues (see Fig. 14.10a–e). The graph "Modal 5" in Fig. 14.12 shows the relative errors of the first 10 eigenfrequencies with this interface reduction. Again the approximation accuracy is improved significantly compared to the interface reduction without the additional interface mode as illustrated by the graph "Modal 4" in Fig. 14.12. The 2nd eigenfrequency is as accurate as without interface reduction and the relative error of the eigenfrequencies is below 1% up to the 5th eigenfrequency. Figure 14.16 shows the shapes of the first 8 eigenmodes corresponding to the lowest eigenvalues of the reduced system. Figure 14.16a–d illustrate that the first 4 eigenmodes correspond to the first 4 eigenmodes of the unreduced system (see also Fig. 14.9a-d) which is confirmed by the MAC values in Fig. 14.14d. Moreover the eigenfrequency of the 1st longitudinal mode (2nd eigenmode) is approximated much better by including the 5th interface modes as can be seen in Fig. 14.12. Furthermore including this 5th interface modes, the 4th eigenmode of the previous section, which shows large interface incompatibilities (Fig. 14.15d), is compensated by this mode and hence disappears or is shifted to higher frequencies. The 3rd bending mode (Fig. 14.16d) is also on the right position now.

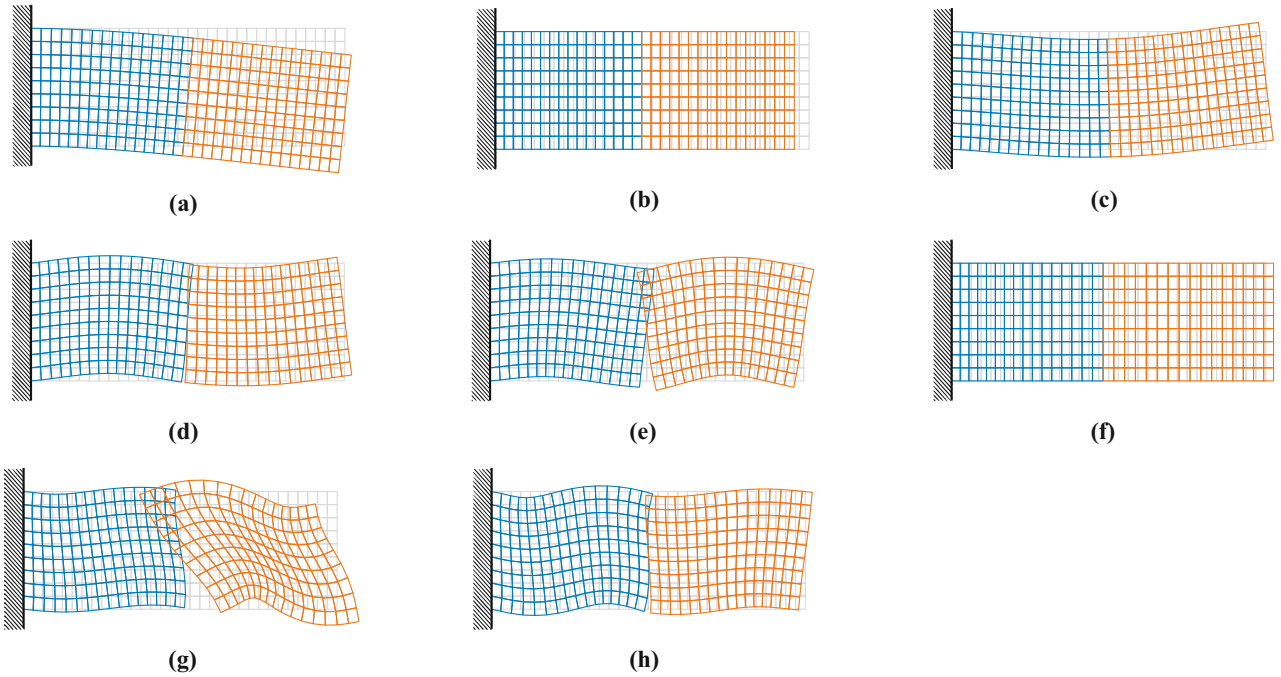

Fig. 14.16 First eight eigenmodes after DCBM ($n_\theta^{(1)} = n_\theta^{(2)} = 8$) with modal interface reduction ($n_{int} = 5$ interface modes kept). (**a**) 1. eigenmode: $\omega^2_{DCB,mod} = 0.0019$. (**b**) 2. eigenmode: $\omega^2_{DCB,mod} = 0.0386$. (**c**) 3. eigenmode: $\omega^2_{DCB,mod} = 0.0398$. (**d**) 4. eigenmode: $\omega^2_{DCB,mod} = 0.1869$. (**e**) 5. eigenmode: $\omega^2_{DCB,mod} = 0.3300$. (**f**) 6. eigenmode: $\omega^2_{DCB,mod} = 0.3479$. (**g**) 7. eigenmode: $\omega^2_{DCB,mod} = 0.6243$. (**h**) (8) eigenmode: $\omega^2_{DCB,mod} = 0.8472$

Considering the 5th interface mode (Fig. 14.10e) it is obvious that this mode only influences longitudinal modes. This explains the improvement of the eigenfrequency of the 1st longitudinal mode as can be seen in Fig. 14.12 when adding this interface mode.

The MAC values in Fig. 14.14d show a high correlation between the 6th eigenmode of the reduced system and the 5th eigenmode of the unreduced system. This mode corresponds to the 2nd longitudinal mode which is represented very good now since the interface incompatibilities are compensated by the additional interface mode. However an eigenmode with high interface incompatibility is on the 5th position now (Fig. 14.16e) which seems to have a certain correlation to the 6th eigenmode of the unreduced system as can be seen in the MAC plot in Fig. 14.14d. According to the MAC values the 7th, 8th and 9th eigenmode of the reduced system corresponds to the 7th, 8th and 9th eigenmode of the unreduced system, respectively. This is obvious for the 8th eigenmode when comparing the mode shapes in Figs. 14.9h and 14.16h and the corresponding eigenvalues are also approximated accurately. High interface incompatibilities are observable for the 5th and 7th eigenmode in Fig. 14.16e, g which have also high relative eigenvalue errors compared to the other values in the low spectrum.

14.5 Conclusions

In this paper two interface reduction techniques for the dual Craig-Bampton method (DCBM) were presented. The modal interface reduction outperforms the static (Guyan) interface reduction when keeping the same number of interface modes but having additional costs since another eigenvalue problem has to be solved. Solving the static condensed interface problem and using the obtained interface normal modes as reduction basis can decrease the number of interface degrees of freedom significantly without deteriorating the approximation accuracy of the eigenfrequencies in the low frequency range. This was shown in an example reducing the remaining 559 degrees of freedom without interface reduction by a subsequent modal interface reduction to 146 degrees of freedom without changing the approximation accuracy of the 20 lowest eigenfrequencies.

Since the number of interface modes corresponding to negative eigenvalues is equal to the number of Lagrange multipliers, the kept interface modes for the reduction have to be chosen with care. It is possible to keep only the interface modes corresponding to positive eigenvalues which has the pleasant side effect that the resulting reduced system does not have any negative eigenvalues anymore which is unavoidable for the DCBM without interface reduction. This could be beneficial in order to avoid possible instabilities occurring when time integrating DCBM reduced systems. Nevertheless keeping only interface modes corresponding to positive eigenvalues decreases the approximation accuracy of the eigenvalues significantly and the corresponding eigenmodes appearing in the low frequency spectrum with high interface incompatibilities do not have any correlation to the eigenmode shapes of the unreduced system. A comprehensible example was used to show that including interface modes corresponding to negative eigenvalues shifts these eigenmodes with high interface incompatibilities out of the low frequency range and therefore improves the approximation accuracy of the eigenvalues. It is recommended to keep interface modes corresponding to negative eigenvalues if the eigenvalues of a system have to be approximated. In future research we plan to study the effect of the interface reduction in the DCBM on the time integration of the reduced system.

References

1. Craig, R.R.: Coupling of substructures for dynamic analyses: an overview. In: Proceedings of AIAA/ASME/ASCE/AHS/ASC Structures, Structural Dynamics, and Materials Conference and Exhibit, Atlanta, pp. 1573–1584 (2000)
2. Craig, R.R., Bampton, M.C.C.: Coupling of substructure for dynamic analyses. AIAA J. **6**(7), 1313–1319 (1968)
3. Craig, R.R., Chang, C.-J.: Substructure coupling for dynamic analysis and testing. Technical report (1977)
4. Craig, R.R., Kurdila, A.J.: Fundamentals of Structural Dynamics. Wiley (2006) ISBN:0471430447
5. Géradin, M., Rixen, D.J.: Mechanical Vibrations: Theory and Application to Structural Dynamics. Wiley (2014) ISBN:1118900197
6. Gruber, F.M., Rixen, D.J.: Evaluation of substructure reduction techniques with fixed and free interfaces. Strojniški vestnik J. Mech. Eng. **62**(7–8), 452–462 (2016). doi: 10.5545/svjme.2016.3735, ISSN:00392480
7. Gruber, F.M., Rutzmoser, J.B., Rixen, D.J.: Comparison between primal and dual Craig-Bampton substructure reduction techniques. In: Moltezar M., Slavic, J., Wiercigroch, M. (eds.) Proceedings of the 11th International Conference on Engineering Vibration, Ljubljana pp. 1245–1254 (2015)
8. MacNeal, R.H.: A hybrid method of component mode synthesis. Comput. Struct. **1**(4), 581–601 (1971). doi: 10.1016/00457949(71)900319, ISSN:00457949
9. Rixen, D.J.: A dual Craig-Bampton method for dynamic substructuring. J. Comput. Appl. Math. **168**(1–2), 383–391 (2004). doi: 10.1016/j.cam.2003.12.014, ISSN:03770427
10. Rixen, D.J.: Dual Craig-Bampton with enrichment to avoid spurious modes. In: Proceedings of IMAC-XXVII (2009)
11. Rixen, D.J.: Interface reduction in the dual Craig-Bampton method based on dual interface modes. In: Proulx, T. (ed.) Linking Models and Experiments, Volume 2: Proceedings of the 29th IMAC, A Conference on Structural Dynamics, 2011, pp. 311–328. Springer, New York (2011). doi: 10.1007/97814419-93052_22, ISBN: 978-1-4419-9305-2
12. Rubin, S.: Improved component-mode representation for structural dynamic analysis. AIAA J **13**(8), 995–1006 (1975). doi: 10.2514/3.60497, ISSN:0001-1452
13. Voormeeren, S.N., Valk, P.L.C. van der, Rixen, D.J.: Generalized methodology for assembly and reduction of component models for dynamic substructuring. AIAA J. **49**(5), 1010–1020 (2011). doi: 10.2514/1.J050724, ISSN:0001-1452